

To appear in the June 2004 issue of *The Astronomical Journal*

L' and *M'* Photometry of Ultracool Dwarfs

D. A. Golimowski,¹ S. K. Leggett,² M. S. Marley,³ X. Fan,⁴ T. R. Geballe,⁵ G. R. Knapp,⁶
 F. J. Vrba,⁷ A. A. Henden,⁷ C. B. Luginbuhl,⁷ H. H. Guetter,⁷ J. A. Munn,⁷ B. Canzian,⁷
 W. Zheng,¹ Z. I. Tsvetanov,⁸ K. Chiu,¹ K. Glazebrook,¹ E. A. Hoversten,¹
 D. P. Schneider,^{9,11} and J. Brinkmann^{10,11}

ABSTRACT

We have compiled *L'* (3.4–4.1 μm) and *M'* (4.6–4.8 μm) photometry of 63 single and binary M, L, and T dwarfs obtained at the United Kingdom Infrared Telescope using the Mauna Kea Observatory (MKO) filter set. This compilation includes new *L'* measurements of 8 L dwarfs and 13 T dwarfs and new *M'* measurements of 7 L dwarfs, 5 T dwarfs, and the M1 dwarf Gl 229A. These new data increase by factors of 0.6 and 1.6, respectively, the numbers of ultracool dwarfs ($T_{\text{eff}} \lesssim 2400$ K) for which *L'* and *M'* measurements have been reported. We compute L_{bol} , BC_K , and T_{eff} for 42 dwarfs whose flux-calibrated *JHK* spectra, *L'* photometry, and trigonometric parallaxes are available, and we estimate these quantities for 9 other dwarfs whose parallaxes and flux-calibrated spectra

¹Department of Physics and Astronomy, The Johns Hopkins University, 3400 North Charles Street, Baltimore, MD 21218-2686

²United Kingdom Infrared Telescope, Joint Astronomy Centre, 660 North A'ohoku Place, Hilo, HI 96720

³NASA–Ames Research Center, Mail Stop 245-3, Moffett Field, CA 94035

⁴Steward Observatory, The University of Arizona, Tucson, AZ 85721-0065

⁵Gemini Observatory, 670 North A'ohoku Place, Hilo, HI 96720

⁶Princeton University Observatory, Princeton, NJ 08544

⁷United States Naval Observatory, Flagstaff Station, P.O. Box 1149, Flagstaff, AZ 86002-1149

⁸National Aeronautics and Space Administration, 300 E Street SW, Washington, DC 20546-0001

⁹Department of Astronomy and Astrophysics, Pennsylvania State University, 525 Davey Laboratory, University Park, PA 16802

¹⁰Apache Point Observatory, 2001 Apache Point Road, P.O. Box 59, Sunspot, NM 88349-0059

¹¹Sloan Digital Sky Survey builder.

have been obtained. BC_K is a well-behaved function of near-infrared spectral type with a dispersion of ~ 0.1 mag for types M6–T5; it is significantly more scattered for types T5–T9. T_{eff} declines steeply and monotonically for types M6–L7 and T4–T9, but is nearly constant at ~ 1450 K for types L7–T4 with assumed ages of ~ 3 Gyr. This constant T_{eff} is evidenced by nearly unchanging values of $L'-M'$ between types L6 and T3. It also supports recent models that attribute the changing near-infrared luminosities and spectral features across the L–T transition to the rapid migration, disruption, and/or thinning of condensate clouds over a narrow range of T_{eff} . The L' and M' luminosities of early-T dwarfs do not exhibit the pronounced humps or inflections previously noted in the I through K bands, but insufficient data exist for types L6–T5 to assert that $M_{L'}$ and $M_{M'}$ are strictly monotonic within this range of types. We compare the observed K , L' , and M' luminosities of L and T dwarfs in our sample with those predicted by precipitating-cloud and cloud-free models for varying surface gravities and sedimentation efficiencies. The models indicate that the L3–T4.5 dwarfs generally have higher gravities ($\log g = 5.0$ – 5.5) than the T6–T9 dwarfs ($\log g = 4.5$ – 5.0). The predicted M' luminosities of late-T dwarfs are 1.5–2.5 times larger than those derived empirically for the late-T dwarfs in our sample. This discrepancy is attributed to absorption at 4.5 – $4.9 \mu\text{m}$ by CO, which is not expected under the condition of thermochemical equilibrium assumed in the models. Our photometry and bolometric calculations indicate that the L3 dwarf Kelu-1 and the T0 dwarf SDSS J042348.57–041403.5 are probable binary systems. We compute $\log(L_{\text{bol}}/L_{\odot}) = -5.73 \pm 0.05$ and $T_{\text{eff}} = 600$ – 750 K for the T9 dwarf 2MASSI J0415195–093506, which supplants Gl 570D as the least luminous and coolest brown dwarf presently known.

Subject headings: infrared: stars — stars: fundamental parameters — stars: late-type — stars: low-mass, brown dwarfs

1. Introduction

The number of known ultracool dwarfs – dwarfs with effective temperatures $T_{\text{eff}} \lesssim 2400$ K – has grown dramatically over the last seven years, primarily because of the sizes and depths of the DEep Near-Infrared Survey of the Southern Sky (DENIS; Epchtein 1997), the Two-Micron All Sky Survey (2MASS; Skrutskie et al. 1997), and the Sloan Digital Sky Survey (SDSS; York et al. 2000). These surveys, and others of lesser scope, have revealed ultracool dwarfs in numbers sufficient to populate a distribution of temperatures ranging from

the coolest hydrogen-burning stars ($1550 \lesssim T_{\text{eff}} \lesssim 1750$ K; Burrows et al. 1993; Chabrier et al. 2000) to the coolest known brown dwarf ($600 \lesssim T_{\text{eff}} \lesssim 750$ K; this paper). Consequently, two new spectral types, L and T, have been defined in order to classify dwarfs cooler than spectral type M (Kirkpatrick et al. 1999b; Martín et al. 1999b; Burgasser et al. 2002a; Geballe et al. 2002, hereafter G02). The spectra of L dwarfs are characterized by absorption from neutral alkali metals (e.g., K, Na, Cs, and Rb) and metallic hydrides (e.g., FeH and CrH) at red wavelengths and by absorption from CO and H₂O at near-infrared wavelengths. In contrast, the optical spectra of T dwarfs are dominated by pressure-broadened K I and Na I absorption lines, and their near-infrared spectra are sculpted by broad absorption bands of CH₄ and H₂O and collisionally-induced absorption (CIA) by H₂.

Most observational studies of ultracool dwarfs concern the spectral region 0.6–2.5 μm . This region is favored because the flux distributions of these objects peak around 1.2 μm and because the spectral sensitivities of modern photoelectronic detectors coincide with the relatively dark and transparent atmospheric windows in this region. Recently, attention has been given to the photometry of ultracool dwarfs longward of the *K* bandpass. This attention has been motivated partly by the need to better constrain the bolometric luminosities of ultracool dwarfs and by the prospects for observing even cooler brown dwarfs or planets at these wavelengths with space-based infrared telescopes. The intrinsic faintness of L and T dwarfs and the increasing brightness and variability of the sky make ground-based observations of these objects in the *L* (2.5–4.0 μm) and *M* (4.1–5.5 μm) bandpasses difficult and time-consuming. Although *L*-band photometry of L and T dwarfs is extensive (Jones et al. 1996; Leggett, Allard, & Hauschildt 1998; Tokunaga & Kobayashi 1999; Stephens et al. 2001; Reid & Cruz 2002; Leggett et al. 2002a, hereafter L02), *M*-band photometry has been published for only six of these objects (Matthews et al. 1996; Reid & Cruz 2002; L02).

Spectroscopic studies of brown dwarfs in the *L* or *M* bandpasses have so far been limited to three L dwarfs and the archetypal T dwarf, Gl 229B. The *L* bandpass contains the Q-branch of the fundamental absorption band of CH₄, which is situated near 3.3 μm . This absorption band appears as early as spectral type L5 ($T_{\text{eff}} \approx 1700$ K; Noll et al. 2000) and is deep and broad in the spectrum of the T6 dwarf Gl 229B ($T_{\text{eff}} \approx 900$ K; Oppenheimer et al. 1998). The *M*-band spectrum of Gl 229B features a broad but shallow absorption trough from 4.5 μm to 4.9 μm and a narrow peak at 4.67 μm , both of which are attributed to the 1-0 vibration-rotation band of CO (Noll, Geballe, & Marley 1997; Oppenheimer et al. 1998). These features reveal a CO abundance that is over 1000 times larger than expected under conditions of CO \leftrightarrow CH₄ thermochemical equilibrium, indicating that CO is rapidly transported outward from warmer, CO-rich layers of the atmosphere (Fegley & Lodders 1996; Griffith & Yelle 1999; Saumon et al. 2000, 2003). The *M*-band fluxes of two other T dwarfs, SDSS J125453.90–012247.4 and 2MASS J05591914–1404488, are reportedly well

below the levels expected for $\text{CO} \leftrightarrow \text{CH}_4$ equilibrium, which suggests that vertical mixing of CO within the atmospheres of T dwarfs is common (L02; Saumon et al. 2003).

In this paper, we present new 3.4–4.1 μm and 4.6–4.8 μm photometry of ultracool dwarfs obtained with the United Kingdom Infrared Telescope (UKIRT) using the Mauna Kea Observatory (MKO) L' and M' filters. These data increase by factors of 0.6 and 1.6, respectively, the numbers of ultracool dwarfs for which MKO L' and M' measurements have been reported. We examine the near-infrared colors and magnitudes of these dwarfs as functions of spectral type. Using recently published trigonometric parallaxes, we show color–magnitude diagrams in the MKO K , L' , and M' bandpasses, and we determine the bolometric luminosities and effective temperatures of ultracool dwarfs. We compare these results with the predictions of recent atmospheric models that consider the effects of cloud sedimentation on the broadband spectra of these objects. Finally, we consider the effects of nonequilibrium $\text{CO} \leftrightarrow \text{CH}_4$ chemistry on the M' luminosities of ultracool dwarfs and on direct searches for even cooler objects at wavelengths around 5 μm .

2. The Sample

The sample of objects under study comprises 63 single and binary M, L, and T dwarfs for which MKO $L'M'$ photometry has been presented by L02, Leggett et al. (2002b), Reid & Cruz (2002), or in this paper. Although our study concerns ultracool dwarfs (spectral types M7 and later), we include in our sample some early-M dwarfs to establish a connection with the cool end of the classical main sequence. Counting only the single dwarfs and the primary components of close binaries, our sample numbers 15 M dwarfs, 28 L dwarfs, and 20 T dwarfs. Table 1 lists the names, multiplicities, spectral types, trigonometric parallaxes, and distance moduli of the dwarfs in our sample, as well as published references for those characteristics. The parallaxes and distance moduli listed in columns 3 and 4 are based upon the weighted means of the parallax measurements referenced in column 6. The names of the dwarfs are the full designations assigned to them by the catalogues or surveys of their origin, using (where possible) the most current naming protocols for those sources. Henceforth, we abbreviate the names of the single and binary dwarfs detected by DENIS, 2MASS, and SDSS using their survey acronyms, followed by the first four digits of both their Julian right ascensions and declinations. These abbreviated forms are preferred by the International Astronomical Union (IAU).

The spectral types of all but two of the L and T dwarfs listed in Table 1 are derived from their J -, H -, and K -band spectra using the near-infrared spectral classification scheme of G02. The types listed for the primary components of close-binary systems are derived from

the composite spectra of the binaries using this classification scheme. The types listed for the secondary components are either previously published estimates or new estimates based on published luminosities and the relationship between luminosity and spectral type presented by L02. The classification scheme of G02 employs four indices that measure the strengths of H₂O and CH₄ absorption bands between 1.1 μm and 2.3 μm . The monotonic variation of these indices through the L and T sequences permits classification of these dwarfs with a typical uncertainty of one-half spectral subtype. The H₂O 1.5 μm index and a fifth index measuring the slope of the red continuum flux are well suited for classifying early-L dwarfs. These indices yield early-L types that are consistent with types obtained from the optical classification schemes of Kirkpatrick et al. (1999b) and Martín et al. (1999b). However, discrepancies between the optical and G02 schemes as large as 2.5 subtypes occur for mid- to late-L dwarfs, which suggests that the optical and near-infrared indices are unequally affected by the changing opacity of condensate clouds as T_{eff} decreases (Stephens 2003). The spectral types of T dwarfs obtained from the independent near-infrared classification schemes of G02 and Burgasser et al. (2002a) usually match within one-half subtype.

We have obtained new MKO L' photometry for 21 dwarfs in our sample (8 L dwarfs and 13 T dwarfs) and new MKO M' photometry for 13 dwarfs in our sample (1 M dwarf, 7 L dwarfs, and 5 T dwarfs). These new data increase to 57 and 21 the numbers of ultracool dwarfs that have been measured photometrically in the MKO L' and M' bandpasses, respectively (L02; Leggett et al. 2002b; Reid & Cruz 2002). This group of ultracool dwarfs is the largest so far measured in any single L - and M -band photometric system. Stephens et al. (2001) obtained L -band photometry of 23 ultracool dwarfs using the L' and L_s filters installed in the Near Infrared Camera (NIRC) at the W. M. Keck Observatory on Mauna Kea, Hawaii. Because no photometric transformations between the Keck L' and L_s bandpasses and the MKO L' bandpass exist yet for ultracool dwarfs, we exclude these 23 measurements from our present analysis.

3. Observations and Data Reduction

The new L' and M' photometric data were obtained between 2001 November and 2003 November using the 3.8 m UKIRT on Mauna Kea, Hawaii. Data obtained before 2002 September 1 were recorded with UKIRT's 1–5 μm InfraRed Camera (IRCAM; Puxley et al. 1994); data obtained thereafter were recorded with the new 1–5 μm UKIRT Imager Spectrometer (UIST; Ramsay-Howat et al. 2000). IRCAM features a 256×256 array of 30 μm InSb pixels and optics that yield a pixel scale of $0''.081 \text{ pixel}^{-1}$ and a field of view of $20''.7 \times 20''.7$. UIST features a 1024×1024 ALADDIN array of 27 μm InSb pixels and

selectable optics in its imaging mode that yield pixel scales of $0''.06 \text{ pixel}^{-1}$ and $0''.12 \text{ pixel}^{-1}$. The former scale and a 512×512 subarray readout were used to increase the efficiency of our observations. This configuration provided a field of view of $30''.7 \times 30''.7$. Both imagers are equipped with broadband filters spanning the range $1.15\text{--}4.9 \mu\text{m}$, including the L' and M' filters of the MKO photometric system (Simons & Tokunaga 2002; Tokunaga, Simons, & Vacca 2002). Descriptions of these filters and the differences between commonly used L - and M -bandpasses have been presented by L02.

To investigate possible differences between the instrumental L' and M' magnitudes of IRCAM and UIST, we synthesized the L' and M' magnitudes of Gl 229B by convolving its $3.0\text{--}4.2 \mu\text{m}$ and $4.5\text{--}5.1 \mu\text{m}$ spectra (Noll, Geballe, & Marley 1997; Oppenheimer et al. 1998) with the measured transmission and reflection profiles of the imagers' optics and detectors. A 5% dip in the $2.7\text{--}3.5 \mu\text{m}$ transmission of UIST's lenses produces a value of L' that is 0.015 mag larger than that computed for IRCAM. No other instrumental features affect the L' magnitudes significantly. The M' magnitudes computed for each imager are nearly identical. The differences between the pairs of synthetic magnitudes are much less than the random errors associated with actual L' and M' magnitudes of ultracool dwarfs obtained with either imager (Table 2). Thus, our limited investigation indicates that L' - and M' -band measurements recorded with IRCAM and UIST are compatible with the MKO L' and M' photometric system.

Table 2 lists the dates and instruments of observation and the calibrated magnitudes of the 28 dwarfs in our sample for which new L' or M' photometric data were obtained. All data were recorded during photometric (dry and cloudless) conditions and subarcsecond seeing. The techniques of recording and reducing the data from both imagers mimicked those of previous IRCAM observations of ultracool dwarfs (L02). Because of the bright sky background, the reduced images comprised scores of short-exposure, co-added frames. Typically, each L' exposure consisted of 100 co-added exposures of 0.2 s, and each M' exposure comprised 75 co-added exposures of 0.12 s. The telescope was offset slightly between frames. Adjacent pairs of frames were subtracted to remove the rapidly varying background signal, and every four pairs of differenced images were combined and divided by a flat field. This process was repeated until the desired ratio of signal to noise (S/N) was achieved. With IRCAM, $S/N \approx 20$ was achieved in 1–30 min for targets having $L' \approx 11\text{--}13$. Likewise, $S/N \approx 10$ was reached in about 1.3 hr for targets having $M' \approx 12$. With UIST, $S/N \approx 15$ was achieved in 1 hr for targets having $L' \approx 13$, and $S/N \approx 13$ was achieved in 1 hr for targets having $M' \approx 11$. All data were calibrated using UKIRT standard stars observed through the MKO L' and M' filters (Leggett et al. 2003).

4. Results and Analysis

Table 3 lists the new and previously published MKO $KL'M'$ photometry for our sample of M, L, and T dwarfs. All measurements come from L02 or this paper unless otherwise noted. Absolute L' magnitudes are also listed for objects whose trigonometric parallaxes have been published. The values of $M_{L'}$ for five T dwarfs are based on the weighted means of absolute parallaxes reported by Dahn et al. (2002, hereafter D02) and Vrba et al. (2004, hereafter V04) and relative parallaxes reported by Tinney, Burgasser, & Kirkpatrick (2003). The $M_{L'}$ for another T dwarf, 2MASS J1534–2952AB, is based solely upon a relative parallax. Tinney, Burgasser, & Kirkpatrick (2003) estimate that the corrections from relative to absolute parallaxes are less than $0''.001$ for their astrometric fields, so the systematic differences between values of $M_{L'}$ derived separately from absolute and relative parallaxes are probably within 0.06 mag for the dwarfs in our sample.

4.1. $K-L'$ and $L'-M'$ colors

Figure 1 shows the variations of $K-L'$ and $L'-M'$ with spectral type for the dwarfs in our sample. The ordinate axes of each diagram have the same incremental scales so that the relative changes in each color may be compared directly. Figure 2 is a diagram of $K-L'$ versus $L'-M'$ for dwarfs measured in all three bandpasses. In these figures, M dwarfs are denoted by circles, L dwarfs by triangles, and T dwarfs by squares. Points representing close-binary systems are surrounded by open circles to distinguish them from single or widely separated dwarfs. These representations are maintained throughout this paper.

The diagram of $K-L'$ versus spectral type is a more populated version of the similar diagram shown by L02. $K-L'$ generally increases monotonically through the spectral sequence, but the rate of increase changes significantly over the range of spectral types shown. The reddening between types M1 and L0 is approximately linear with a dispersion of ~ 0.06 mag, but $K-L'$ increases nonlinearly through the L sequence with a dispersion of ~ 0.15 mag. This scatter has been attributed to the strong and varying effects of condensate clouds on the emergent K - and L -band fluxes over the associated range of T_{eff} (Ackerman & Marley 2001; L02). Variations in surface gravity among L dwarfs may also contribute to this scatter (see §5). The nearly unchanging values of $K-L'$ between types L6 and T5 were noted by L02, who attributed this behavior to the balanced effects of increasing CH_4 absorption at 2.2–2.4 μm and 3.3–3.7 μm , the latter of which extends into the blue half of the L' band. Similar behavior can be inferred from the Keck $K-L'$ measurements of Stephens et al. (2001) despite a lack of data for types L8.5–T0.5. As we discuss in §4.3, this behavior may also reflect the redistribution of flux caused by the settling of condensate clouds in the photosphere.

The rapid increase of $K-L'$ beyond type T5 may be caused by increasing H_2 CIA in the K band, saturation (or, alternatively, weakening) of the CH_4 absorption band at 3.3–3.7 μm , or both. The L9 dwarf with the anomalously blue $K-L' = 1.20$ is SDSS J0805+4812, and the T6 dwarf with the anomalously red $K-L' = 3.05$ is 2MASS J0937+2931. We discuss these dwarfs in §4.5.

$L'-M'$ decreases slowly between spectral types M5 and L6, probably because of strengthening CO absorption at 4.5–4.9 μm (Tsuji & Ohnaka 1995; Tsuji, Ohnaka, & Aoki 1995; Reid & Cruz 2002). The color is nearly constant between types L6 and T3, which suggests that the varying absorptions by CH_4 at 3.3–3.7 μm and CO at 4.5–4.9 μm have balanced effects on the integrated L' and M' fluxes, or that T_{eff} changes little within this range of spectral types. While the former condition may be true, the results presented in §4.3 indicate that the latter condition is certainly true. Beyond type T5, $L'-M'$ rises steeply, i.e. it becomes significantly redder. This reddening cannot be definitively explained without a representative collection of L - and M -band spectra. It may be caused by dissipating CO absorption at 4.5–4.9 μm , or it may simply reflect a Wien-like shift of the spectral energy distribution as T_{eff} decreases.

4.2. Color–magnitude and magnitude–spectral type relations

Figures 3a and 3b are color–magnitude diagrams (CMDs) of M_K versus $K-L'$ and $K-M'$, respectively, for the dwarfs in our sample. Figure 3a is similar to the M_K versus $K-L'$ diagram presented by L02, but it shows many more data, especially in the T dwarf domain $1.5 < K-L' < 2.5$. Figure 3b greatly extends the equivalent $M_{M'}$ versus $K-M'$ diagram of Reid & Cruz (2002) by including L and T dwarfs with $0.7 \lesssim K-M' \lesssim 3.7$. The bright end of each diagram represents the M1 dwarf Gl 229A; the faint end represents the T9 dwarf 2MASS J0415–0935. We cannot explain in detail the characteristics of these CMDs without a comprehensive set of 3.4–4.8 μm spectra, but their basic appearances are significant. The anomalous 2MASS J0937+2931 notwithstanding (see §4.5), both diagrams are monotonic throughout the M, L, and T spectral classes. Such monotonicity, combined with a wide range of color values, is rare among CMDs constructed from combinations of optical and near-infrared bandpasses. For example, the reversals of $J-H$ and $H-K$ caused by strengthening CH_4 absorption at 1.6–1.8 μm and 2.2–2.4 μm (G02; Burgasser et al. 2002a) cause degeneracies in the JHK -based CMDs of M and early-T dwarfs (L02; D02; Tinney, Burgasser, & Kirkpatrick 2003; V04; Knapp et al. 2004, hereafter K04). Combinations of I -, J -, and K -band measurements produce CMDs that are similarly degenerate over a wide range of spectral types (Tinney, Burgasser, & Kirkpatrick 2003). CMDs constructed exclusively

from SDSS i and z photometry are monotonic for $i-z \lesssim 5.2$, but SDSS measurements of late-T dwarfs with known distances are presently lacking (Hawley et al. 2002; K04). Consequently, Figures 3a and 3b are the only CMDs with sufficient range and resolution to enable reliable estimates of photometric parallaxes throughout the presently defined L and T sequences.

We have derived parametric expressions for each CMD by computing least-squares fits of polynomials to their respective data. Because the intrinsic scatter of the data exceeds the photometric and astrometric measurement errors, the data were not weighted. Data representing close-binary systems and 2MASS J0937+2931 were excluded from the fits. The curves in Figures 3a and 3b are low-order polynomials that yield the optimum χ^2 statistic for the selected range of data. The coefficients and residual statistics of the fits are listed in Table 4. The fits are intended primarily for estimating the luminosities and distances of individual dwarfs from MKO $KL'M'$ photometry. Because the data represent dwarfs of unknown multiplicity and age, the fits can be used to derive only a provisional luminosity function for ultracool dwarfs.

Figures 4a and 4b are diagrams of $M_{L'}$ and $M_{M'}$ as functions of spectral type. These diagrams complement the diagrams presented by Tinney, Burgasser, & Kirkpatrick (2003) and K04 for MKO J and K photometry reported by L02 and K04.¹² The curves in Figures 4a and 4b are low-order polynomials fitted to the unweighted data, excluding those for known close binaries. The coefficients and residual statistics of these fits are listed in Table 4. The fits are not χ^2 -optimal, but they provide means of estimating the luminosities and distances of M, L, and T dwarfs for which MKO $L'M'$ photometry and near-infrared spectral types have been obtained. The combination of $L'M'$ photometry with JHK -based spectral types seems awkward, but the relatively small scatter in the L' and M' luminosities – especially among types L0 to L5 – provides an advantage over combinations of JHK photometry and optical or near-infrared spectral types (L02; D02; Tinney, Burgasser, & Kirkpatrick 2003; V04; K04).

The fits in Figures 4a and 4b indicate that $M_{L'}$ and $M_{M'}$ decrease monotonically throughout the M, L, and T classes. They do not exhibit the pronounced “hump” or inflection in luminosity noted for early-T dwarfs in diagrams of M_{IC} , M_Z , M_J , M_H , and M_K

¹²Tinney, Burgasser, & Kirkpatrick (2003) incorrectly described L02’s J and K data as having been measured on the old UKIRT photometric system instead of the proper MKO system. Also, Tinney, Burgasser, & Kirkpatrick (2003) employed L types derived from the optical classification scheme of Kirkpatrick et al. (1999b) rather than the near-infrared scheme of G02 used by us. The two schemes often yield discordant mid-L to early-T types, so systematic inconsistencies between our Figure 4 and the diagrams of Tinney, Burgasser, & Kirkpatrick may exist for these types.

versus spectral type (Tinney, Burgasser, & Kirkpatrick 2003; V04; K04). The amplitude of this feature increases from I_C to J (Tinney, Burgasser, & Kirkpatrick 2003) and decreases from J to K (V04; K04). The lack of obvious humps or inflections in Figures 4a and 4b suggests that the latter trend continues through the L' and M' bands. Close inspection of Figure 4a shows that the polynomial fit may overestimate by ~ 0.5 mag the values of $M_{L'}$ for early-T dwarfs, but more L' and parallax measurements of T0–T5 dwarfs are needed to confirm this possibility. No inflection appears in Figure 4b, but insufficient data exist for types L6–T5 to assert with confidence that $M_{M'}$ is strictly monotonic within this range of types.

The apparently monotonic decrease of the L' and M' luminosities with decreasing T_{eff} is consistent with recent explanations of the “early-T hump” at shorter wavelengths. Using models of precipitating condensate clouds, Ackerman & Marley (2001) and Marley et al. (2002) showed that a horizontally-uniform cloud deck forms progressively deeper in the atmosphere and becomes more optically thick as T_{eff} decreases. This behavior significantly affects the z - through K -band fluxes of late-L and early-T dwarfs ($T_{\text{eff}} \approx 1450$ K; see §4.3), but it affects much less the emergent flux outside these bandpasses. The migration of the cloud deck into the convective region of the atmosphere may also disrupt the deck’s uniformity, thereby allowing more J -band flux from hotter layers of the atmosphere to escape through holes in the clouds (Ackerman & Marley 2001; Burgasser et al. 2002b). Alternatively, the efficiency of sedimentation may rapidly increase at the L–T transition and enhance the J -band flux (K04). Tsuji & Nakajima (2003) also attributed the L–T transition to the inward migration of thin dust clouds as T_{eff} decreases, but they viewed the reported brightening of the J -band flux as an artifact of a small sample of brown dwarfs with different masses, ages, and cooling tracks. They did not extend their demonstration to shorter or longer wavelengths, but Tsuji (2002) reported that the effect of cloud migration on the emergent spectrum is largest in the J band. Whether or not cloud migration alone is sufficient to explain the sudden appearance of the “early-T hump”, the dynamics of the cloud deck below $T_{\text{eff}} \approx 1400$ K have comparatively little impact on the emergent L' and M' fluxes. The predicted effects of temperature, clouds, and gravity on $M_{L'}$ and $M_{M'}$ are examined further in §5.

4.3. Bolometric Luminosities and Effective Temperatures

Our large and comprehensive set of L' measurements permits us to determine with reasonable accuracy the bolometric luminosities (L_{bol}) and T_{eff} of ultracool dwarfs. We have computed and compiled L_{bol} of 42 dwarfs in our sample for which flux-calibrated spectra, L' photometry, and trigonometric parallaxes are available. To this group, we have added nine

M, L, and T dwarfs for which spectra and *JHK* photometry exist and for which trigonometric parallaxes have recently been measured. The L' luminosities of these supplemental dwarfs can be estimated from the measured L' magnitudes of dwarfs in our sample that have similar spectral types and *JHK* colors (K04). The names, spectral types, parallaxes, and magnitudes of these nine dwarfs are listed in Table 5 along with their respective references.

As a first step toward computing L_{bol} , we used SDSS *iz*, UKIRT *Z*, and MKO *JHK* photometry (L02; K04) to calibrate the 0.8–2.5 μm spectra (Leggett et al. 1999; G02; Burgasser et al. 2002a; K04) of the 51 dwarfs under study. We also used our MKO L' and M' measurements of Gl 229B to calibrate its 3.0–4.2 μm and 4.5–5.1 μm spectra (Noll, Geballe, & Marley 1997; Oppenheimer et al. 1998). For Gl 229B, we summed the available spectra from *I* through *M* bands, linearly interpolated the fluxes in the regions 2.5–3.0 μm and 4.2–4.5 μm , and assumed a Rayleigh–Jeans (R–J) flux distribution longward of *M*. The R–J approximation is compromised by the presence of absorption by CH_4 , H_2O , and NH_3 between 6 and 11 μm (Marley et al. 1996; Burrows et al. 2001), but we estimate that this absorption decreases by $\lesssim 1\%$ the bolometric flux of dwarfs with $T_{\text{eff}} \gtrsim 600$ K (Burrows et al. 2001). For the other dwarfs, we summed the spectra from their blue limits through *K* band, interpolated the flux between *K* and the effective L' flux computed from our photometry, and assumed a R–J distribution longward of L' . Neither the interpolation between *K* and L' nor the R–J extrapolation longward of L' is valid for T dwarfs, because CH_4 absorbs shortward of L' and CO absorbs significantly in *M*. Consequently, we used the summed *L*- and *M*-band spectra of Gl 229B to determine corrections for these approximations. The corrections *increase* by 20% the derived bolometric fluxes of mid- to late-T dwarfs. (The absorption by CH_4 and CO is more than offset by the flux beyond L' that exceeds our R–J approximation.) Leggett et al. (2001) used model atmospheres to determine that no correction is needed for late-M to mid-L dwarfs. For types L8–T3.5, we adopted a correction that is half that computed for the later T dwarfs. We applied these corrections to the fluxes of the mid-L to late-T dwarfs, verifying where possible the bolometric fluxes derived from this method against those computed using our M' measurements and an R–J approximation longward of M' . We found that the two methods matched within $\sim 5\%$. We estimate that the uncertainties in the bolometric fluxes of all the dwarfs are 5–11%.

We used the magnitudes obtained from our bolometric fluxes and the *K* photometry of L02 and K04 to compute *K*-band bolometric corrections (BC_K) for the 51 M, L, and T dwarfs in our supplemented sample. We also used the weighted-mean parallaxes listed in Tables 1 and 5 to convert the bolometric fluxes into L_{bol} and compute absolute bolometric magnitudes (M_{bol}). Table 6 lists L_{bol} [expressed as $\log(L_{\text{bol}}/L_{\odot})$], M_{bol} , and BC_K for the 51 dwarfs. Many of these quantities are based on photometry and astrometry reported since the work of L02 (D02; Tinney, Burgasser, & Kirkpatrick 2003; V04; K04; this paper), so the

information in Table 6 supersedes that given in Table 7 of L02.

We used the relationships between L_{bol} and T_{eff} derived from the evolutionary models of Burrows et al. (1997), Baraffe et al. (1998), and Chabrier et al. (2000) to obtain T_{eff} for the dwarfs listed in Table 6. Because the radii of brown dwarfs older than 0.1 Gyr vary by no more than 30% (Marley et al. 1996; Burrows et al. 2001), the range of possible T_{eff} for a given L_{bol} remains within ~ 300 K regardless of mass or age. This behavior is illustrated in Figure 5, which shows the relationships between L_{bol} and T_{eff} predicted by the models of Burrows et al. (1997) and Chabrier et al. (2000). Column 6 of Table 6 lists the range of T_{eff} derived from the values of L_{bol}/L_{\odot} listed in Column 5, assuming ages of 0.1–10 Gyr.¹³ Column 7 lists T_{eff} for an age of ~ 3 Gyr (unless otherwise noted), which represents the mean age of nearby brown dwarfs inferred from their kinematics (D02). These values of T_{eff} supersede those reported by L02 for dwarfs common to both samples. The broad range of assumed ages contributes uncertainties of $\sim 10\%$ to T_{eff} . For dwarfs whose computed values of L_{bol} have errors within 10%, the contributions of these errors to the uncertainties in T_{eff} are 1–2.5%. Thus, the uncertainties in T_{eff} for dwarfs whose measured parallaxes have errors $\lesssim 5\%$ are dominated by our conservative range of ages for the dwarfs. A less conservative range of 0.5–10 Gyr increases the minimum T_{eff} for each dwarf by ~ 200 K.

Figures 6a and 6b are diagrams of BC_K and T_{eff} versus spectral type for the M6–T9 dwarfs listed in Table 6. The plotted values of T_{eff} are those listed in Column 7 of the table for a mean age of ~ 3 Gyr, except where noted. The error bars for these values reflect the full ranges of T_{eff} listed in Column 6 of the table. The curves in Figures 6a and 6b are nonoptimal fourth- and sixth-order polynomials fitted to the weighted data, excluding the data for known close binaries. The datum for the anomalous T6 dwarf 2MASS 0937+2931 (see §4.5) is omitted from in Figure 6a for clarity’s sake, but it is included in the polynomial fit to the data. The fit in Figure 6b is fixed at type T9 to avoid an unrealistic upturn in T_{eff} between types T8 and T9. The coefficients and residual statistics of these fits are listed in Table 4.

The fitted curve in Figure 6a shows that BC_K is a piecewise-monotonic function of spectral type with a small dispersion (~ 0.1 mag) for types M6–T5. The increased dispersion

¹³The ages of some dwarfs have been further constrained by assuming coevality with their main sequence companions whose ages have been delimited observationally. These systems are: Gl 229AB (0.5–10 Gyr; Nakajima et al. 1995; J. Stauffer 2001, personal communication; Leggett et al. 2002b; Gizis, Reid, & Hawley 2002; I. N. Reid 2003, personal communication), LHS 102AB (1–10 Gyr; Leggett et al. 2002b; Gizis, Reid, & Hawley 2002), GD 165B (1.2–5.5 Gyr; Kirkpatrick et al. 1999a), Gl 584C (1–2.5 Gyr; Kirkpatrick et al. 2001), and Gl 570D (2–5 Gyr; Burgasser et al. 2000; Geballe et al. 2001). Also, the age of Kelu-1 has been constrained to 0.3–1 Gyr on the basis of its Li I $\lambda 6708$ Å absorption strength (Basri et al. 1998).

for the late-T dwarfs may indicate the sensitivity of H₂ CIA, which significantly affects the *K*-band spectrum, to variations in surface gravity (Saumon et al. 1994; Burgasser et al. 2002a; K04). BC_{*K*} gradually rises between types M5 and L5, which is expected from Wien’s law but may also indicate enhanced *K*-band luminosity as the cloud deck settles below the “*K*-band photosphere” (1500 ≲ *T*_{eff} ≲ 1400 K; Ackerman & Marley 2001; Marley et al. 2002). BC_{*K*} generally declines for types later than L5, which reflects the increasing strength of combined absorption by CH₄ at 2.2–2.4 μm and CO at 2.3–2.5 μm (G02; Burgasser et al. 2002a).

Figure 6b shows that *T*_{eff} declines steeply and monotonically for types M6–L7 and T4–T9. The decline from L0 to L7 (2300 ≳ *T*_{eff} ≳ 1450 K, for assumed ages of ∼ 3 Gyr) is nearly linear, as noted by Stephens et al. (2001). *T*_{eff} is approximately constant (∼ 1450 K) for types L7–T4, which lie within the range of types for which *K*–*L*′ and *L*′–*M*′ appear constant (Figure 1). This coincidence suggests that the constancy of *T*_{eff} is the cause for these unchanging colors, but the substantial changes in the *K*-band spectra of these brown dwarfs (G02; Burgasser et al. 2002a) show that their spectral energy distributions are not static at ∼ 1450 K. Indeed, the constancy of *T*_{eff} for types L7–T4 is not evident in diagrams of *z*–*J*, *J*–*H*, and *H*–*K* versus spectral type (L02; Burgasser et al. 2002a; Hawley et al. 2002; K04). These colors increase or decrease substantially over this range. The dichotomy between these changing colors and the nearly constant *K*–*L*′ and *L*′–*M*′ between types L6 and T5 may be attributed to the migration and disruption of condensate clouds deep in the photosphere (Ackerman & Marley 2001; Marley et al. 2002; Burgasser et al. 2002b; Tsuji 2002; Tsuji & Nakajima 2003). These cloud dynamics occur over a narrow range of *T*_{eff}¹⁴ and significantly affect only the 0.9–2.5 μm region of the flux spectrum. Consequently, *L*′–*M*′ should not vary significantly across the L–T boundary. Nevertheless, the small decrease in the *L*′ and *M*′ luminosities between types L6 and T5 (Figure 4) suggests that some redistribution of spectral energy from 3.5–5.0 μm to shorter wavelengths occurs as the cloud deck settles or disrupts. Thus, the constancy of *K*–*L*′ may be attributed to the balanced effects of enhanced *K*-band flux and increased CH₄ absorption at 2.2–2.4 μm, both of which occur rapidly as the cloud deck sinks, and gradually decreasing *L*′ luminosity.

Figures 7a and 7b show the variations of BC_{*K*} with MKO *J*–*K* and *K*–*L*′. The data for

¹⁴Burgasser et al. (2002b) reproduced the 2MASS magnitudes and colors of L and T dwarfs by assuming that the cloud deck disrupts rapidly at *T*_{eff} ≈ 1200 K. Likewise, K04 showed that the MKO *J* and *K* CMDs of L–T transition dwarfs are bounded by the 1300 K isotherms that connect the color–magnitude sequences predicted by cloudy and cloud-free models for a wide range of gravity. These transition temperatures are ∼ 10–15% lower than the *T*_{eff} ≈ 1450 K that we compute empirically for L7–T4 dwarfs using the effective temperatures at age ∼ 3 Gyr listed in Table 6.

2MASS 0937+2931 are again omitted from the figures for clarity’s sake. These diagrams are augmented versions of ones shown by L02, and employ new J photometry reported by K04. BC_K is neither a monotonic nor single-valued function of $J-K$ because of the color reversal brought on by increasing CH_4 absorption at 2.2–2.4 μm for types L8 and later (G02). BC_K is a better behaved function of $K-L'$, but it is degenerate for $K-L' \approx 1.6$. This degeneracy reflects the balanced effects of flux redistribution and CH_4 absorption in the K - and L' -bands for L6–T5 dwarfs. Thus, Figures 7a and 7b are not useful stand-alone references for bolometric luminosities near the L–T boundary.

4.4. Comparison of Effective-Temperature Scales

Since the initial discoveries of numerous L dwarfs by DENIS and 2MASS, many estimates of the relationship between T_{eff} and L subtype have been reported. Kirkpatrick et al. (1999b) and Reid et al. (1999) offered initial estimates of the T_{eff} scale of L dwarfs by comparing the evolutions of absorption features in their optical spectra with chemical-equilibrium abundance profiles predicted for the atoms and molecules responsible for those features (Burrows & Sharp 1999). Martín et al. (1999b) and Basri et al. (2000) derived a warmer T_{eff} scale by fitting synthetic absorption profiles of Rb I $\lambda 7948 \text{ \AA}$ and Cs I $\lambda 8521 \text{ \AA}$ with those observed in their optical spectra. Noll et al. (2000), Leggett et al. (2001), and Schweitzer et al. (2002) also developed T_{eff} scales for L dwarfs by fitting model spectra to their sets of optical and near-infrared spectra. Consequently, the accuracy of each T_{eff} scale is tied to the fidelity of the contemporaneous model atmospheres on which the scale is based. Differences among these scales probably reflect the rapidly evolving details of the model atmospheres rather than fundamentally different perspectives on the effective temperatures of ultracool dwarfs. Fortunately, empirically-based T_{eff} scales have been derived that are immune to the idiosyncracies of model atmospheres and depend only on the comparatively robust theoretical relationship between the ages and radii of brown dwarfs (Leggett et al. 2001; L02; D02; V04; this paper). We now compare the effective temperatures listed in Table 6, which supersede the results of Leggett et al. (2001) and L02, with the empirical T_{eff} scales derived by D02 and V04.

D02 derived T_{eff} for 17 M and L dwarfs listed in Table 6.¹⁵ In doing so, they applied the

¹⁵The 17 dwarfs are LHS 3003 (M7), LHS 2065 (M9), BRI 0021–0214 (M9.5), 2MASS J0345+2540 (L1), 2MASS J1439+1929 (L1), 2MASS J0746+2000AB (L1 + \sim L2), DENIS J1058–1548 (L3), GD 165B (L3), Kelu-1 (L3), 2MASS J2224–0158 (L3.5), 2MASS J0036+1821 (L4), LHS 102B (L4.5), 2MASS J1507–1627 (L5.5), DENIS J0205–1159AB (L5.5 + L5.5), 2MASS J0825+2115 (L6), DENIS J1228–1547AB (L6 + \sim L6), and 2MASS J1632+1904 (L7.5).

$BC_{K_{\text{UKIRT}}}$ versus $I_{\text{C}}-K_{\text{UKIRT}}$ relation of Leggett et al. (2001) to their collection of JHK photometry measured on the California Institute of Technology (CIT) and 2MASS photometric systems. They also adopted radii that are halfway between those predicted by the models of Burrows et al. (1997) and Chabrier et al. (2000) for their resultant values of M_{bol} and assumed ages of 1–5 Gyr. The values of T_{eff} derived by D02 for the eleven M7–L4.5 dwarfs are higher by an average of ~ 60 K than those listed in Column 7 of Table 6 for the same dwarfs. Conversely, the values derived by D02 for the five L5.5–L7.5 dwarfs are lower by an average of ~ 30 K than the corresponding values in Table 6. Although these discrepancies lie within the ranges of uncertainty of both T_{eff} scales, their systematic nature is likely due to slightly different applications of the evolutionary models for particular combinations of luminosity and age. We discount the possibilities that these differences are caused by discordant photometric measurements or improper use of the UKIRT bolometric corrections by D02.

The ranges of T_{eff} computed by D02 for the 17 dwarfs are approximately half as wide as those listed in Column 6 of Table 6 for the same dwarfs. D02’s smaller uncertainties are not the result of more accurate data, but instead reflect the 1–5 Gyr range of ages assumed for all the dwarfs in their sample. This range is much narrower than our adopted range of 0.1–10 Gyr for the dwarfs listed in Table 6 whose ages cannot be constrained by the ages of stellar companions. By assuming a lower age limit of 1 Gyr, D02 eliminate from consideration the era in which the radii of ultracool dwarfs change greatly and rapidly (Burrows et al. 1997; Chabrier et al. 2000). The possible youth of Kelu-1 and Gl 229B¹³ suggest that the 1–5 Gyr range of ages assumed by D02 is too narrow to encompass a random sample of ultracool dwarfs in the solar neighborhood. In general, the ranges of ages assumed for such samples must be carefully considered when comparing T_{eff} scales derived from structural models. Figure 5 shows that, for a fixed L_{bol} , narrowing the age range from 0.1–10 Gyr to 1–5 Gyr compresses the corresponding range of T_{eff} asymmetrically so that its midpoint shifts to a higher T_{eff} than would be expected if the radii of brown dwarfs decreased uniformly over time. Consequently, comparisons of T_{eff} scales must be based on temperatures derived for some fiducial age or radius, rather than the midpoint of the T_{eff} range. Otherwise, discrepancies between T_{eff} scales might be declared where none actually exists.

V04 applied our polynomial fit of BC_K versus spectral type (Table 4) to a sample of 56 L and T dwarfs whose trigonometric parallaxes have been measured at the United States Naval Observatory (D02; V04). In doing so, they assumed equality between the dwarfs’ K magnitudes, which were collected from different sources and transformed to approximate K_{CIT} magnitudes, and the K_{MKO} magnitudes on which our bolometric corrections are based. V04 also employed spectral types based on the optical L-dwarf classification scheme of Kirkpatrick et al. (1999b) and the near-infrared T-dwarf classification scheme of Burgasser et al.

(2002a), rather than the near-infrared classification scheme of G02 that defines our L and T subtypes. Despite the noted differences between the CIT and MKO photometric systems (Stephens & Leggett 2004) and the optical and near-infrared classification schemes (Stephens 2003), the values of $\log(L_{\text{bol}}/L_{\odot})$, M_{bol} , and T_{eff} obtained by V04 are generally consistent with those shown in Table 6 for the dwarfs common to both studies. However, significant differences exist for some individual dwarfs and spectral types. For instance, our ranges of T_{eff} for early-L dwarfs are 100–400 K cooler than those of V04. This discrepancy is caused by the fixed range of radii (0.075–0.105 R_{\odot}) adopted by V04 for all the dwarfs in their sample. Imposing a less conservative, but more appropriate, lower limit of $\sim 0.1 R_{\odot}$ upon dwarfs with $\log(L_{\text{bol}}/L_{\odot}) \gtrsim -4.5$ (Burrows et al. 1997; Chabrier et al. 2000) brings V04’s T_{eff} scale for early-L dwarfs into agreement with ours. V04 computed $\log(L_{\text{bol}}/L_{\odot}) = -5.58 \pm 0.10$ and $T_{\text{eff}} = 764^{+88}_{-71}$ K for the T9 dwarf 2MASS J0415–0935. These values are significantly higher than the corresponding values in Table 6. The discrepancies are due to a 0.4-mag difference between our measured K_{MKO} magnitude and the transformed K_{CIT} magnitude adopted by V04. The 0.4-mag difference is probably caused by the 20% uncertainty in the measured 2MASS K_s magnitude of 2MASS J0415–0935 and the ~ 0.2 -mag systematic error for late-T dwarfs associated with the 2MASS-to-CIT transformation employed by V04 (Stephens & Leggett 2004). Nevertheless, the possibility that 2MASS J0415–0935 is photometrically variable cannot be excluded.

4.5. Noteworthy L and T dwarfs

Several ultracool dwarfs in our sample merit special consideration. We describe them here, in progressive order of spectral type.

Kelu-1 (L3) is ~ 1 mag more luminous in L' and M' than the other L3 dwarfs in our sample. Similar overluminosity in other bandpasses is well documented (Martín et al. 1999b; Leggett et al. 2001). Kelu-1’s large rotational velocity (60 ± 5 km s $^{-1}$; Basri et al. 2000) and periodic photometric variability (Clarke, Tinney, & Covey 2002) suggest possible duplicity, but no companion has yet been imaged (Martín, Brandner, & Basri 1999a). Kelu-1’s age has been constrained to 0.3–1 Gyr based on the strength of Li I $\lambda 6708$ Å absorption (Basri et al. 1998). For this range of ages, our computed L_{bol} yields $T_{\text{eff}} = 2100$ –2350 K. These temperatures are ~ 400 K hotter than those of the other L3 dwarfs. For Kelu-1 to have a T_{eff} consistent with the other L3 dwarfs, it must have a mass of $\sim 0.012 M_{\odot}$ and an age of ~ 10 Myr (Burrows et al. 1997). This age is inconsistent with the lower bound set by the Li I absorption, and Kelu-1 is not located near a known region of star formation (Ruiz, Leggett, & Allard 1997). Moreover, Kelu-1 exhibits H α emission, which is characteristic of

old, early-L dwarfs (Gizis et al. 2000). These conditions don’t preclude the possibility that Kelu-1 is extremely young, but the collective evidence favors unresolved duplicity as the cause of Kelu-1’s overluminosity.

2MASS J2244+2043 (L7.5) has a $K-L'$ color that is ~ 0.3 mag redder than those of other late-L dwarfs. D02 reported that its 2MASS $J-K_s$ color is $\gtrsim 0.5$ mag redder than those of all other L dwarfs in their sample. K04 reported that the MKO $J-H$ and $H-K$ colors of 2MASS J2244+2043 are significantly redder than those of other L dwarfs whose spectral types lie within the broad range (L5.5–L9.5) spanned by the near-infrared spectral indices (G02) computed for 2MASS J2244+2043. K04 suggested that the anomalous JHK colors may be caused by condensate clouds that are more optically thick than usual. A comprehensive set of J - through L -band spectra of 2MASS J2244+2043 is needed to determine whether unusually opaque clouds or other conditions cause the excessively red colors throughout these bands.

SDSS J0805+4812 (L9) is an anomalously blue ($K-L' = 1.20$) late-L dwarf. K04 reported that its $J-H$ and $H-K$ colors are ~ 0.2 – 0.3 mag bluer than those of other dwarfs whose spectral types lie within the L7.5–T0.5 range spanned by the indices (G02) computed for SDSS J0805+4812. Its 1.0–2.5 μm spectrum reveals unusually strong H_2O , K I, and FeH absorption, which suggests that the atmosphere of SDSS J0805+4812 is relatively free of condensate clouds or metal-poor (K04). The former possibility is inconsistent with the observed value of $K-L'$, however, because a cloudless atmosphere with $T_{\text{eff}} \approx 1400$ K should yield a redder value of $K-L'$ than a corresponding cloudy atmosphere (see §5). A comprehensive set of J - through L -band spectra is needed to determine the cause(s) of the unusual colors of SDSS J0805+4812.

SDSS J0423-0414 (T0) is ~ 1 mag more luminous in L' and M' than other dwarfs of similar spectral type in our sample. Overluminosities of ~ 0.75 – 1.5 mag in J , H , and K have also been reported by V04 and K04. SDSS J0423-0414 is not known to be multiple. V04 state that its JHK colors and luminosities better suit its optical spectral type of L7.5 (Cruz et al. 2003) than its near-infrared spectral type of T0 (G02). This contradiction may be virtual, however, because the spectral classification schemes of Kirkpatrick et al. (1999b) and G02 are not rigidly correlated for late-L and early-T dwarfs. Unfortunately, $K-L'$ and $L'-M'$ are nearly constant for near-infrared types L7–T4 (Figure 1), so these colors do not constrain SDSS J0423-0414’s spectral type. However, Figures 4a and 4b show that the L' and M' overluminosities of this dwarf are the same whether it has a near-infrared type of L7.5 or T0. Moreover, Table 6 and Figure 6a show that the BC_K computed for SDSS J0423-0414 is more consistent with type T0 than type L7.5. Thus, our photometry and derived BC_K support the T0 classification assigned to SDSS J0423-0414 by G02 on the basis of its highly consistent near-infrared spectral indices. Our results do not refute the L7.5 optical

classification; they merely reflect the dominant contribution of the dwarf’s near-infrared flux to its bolometric flux. Our computed L_{bol} for SDSS J0423–0414 yields $T_{\text{eff}} = 1450\text{--}1825$ K for assumed ages of 0.1–10 Gyr. These temperatures are ~ 300 K hotter than those of other dwarfs with types L9–T1 (Table 6). For SDSS J0423–0414 to have a T_{eff} consistent with the other L9–T1 dwarfs, it must have a mass of $\sim 0.009 M_{\odot}$ and an age of ~ 3 Myr (Burrows et al. 1997). Burgasser et al. (2003a) speculate that SDSS J0423–0414 is an older, more massive T dwarf because it exhibits $\text{H}\alpha$ emission and it has an optical continuum whose slope is consistent with relatively large surface gravity. Moreover, SDSS J0423–0414 does not lie near a known star-forming region. Thus, the collective evidence indicates that SDSS J0423–0414’s overluminosity is likely caused by unresolved multiplicity rather than extreme youth. Its putative components probably have equal masses, because a coeval companion of lesser mass would have $T_{\text{eff}} \lesssim 1450$ K and a spectral type later than T4 (Figure 6b). SDSS J0423–0414’s near-infrared spectrum does not exhibit such heterogeneity (G02).

2MASS J0559–1404 (T4.5) was reported by D02 to be ~ 1 mag more luminous in J than the L8 dwarfs Gl 337C, Gl 584C, and 2MASS J1632+1904. *Hubble Space Telescope* observations revealed no bright companion beyond $0''.05$ of the T dwarf (Burgasser et al. 2003c). Our L' and M' measurements indicate that 2MASS J0559–1404 is no more luminous than the upper bound of the intrinsic scatter observed for the T dwarfs. This conclusion agrees with that of V04, who find that the J , H , and K luminosities of 2MASS J0559–1404 are consistent with the “early-T hump.”

2MASS J0937+2931 (T6) has an anomalously red color of $K-L' = 3.05$. Its $M_{L'}$ is consistent with those of other T6 dwarfs (Table 3), so its overly red $K-L'$ can be attributed to its suppressed K -band flux caused by uncommonly strong H_2 CIA (Burgasser et al. 2002a). Such strong absorption may be attributed to high surface gravity ($\log g > 5.5$; K04) or to low metallicity (Saumon et al. 1994; Burgasser et al. 2002a; K04). Either condition may also account for the absence of the K I absorption doublet at $1.24 \mu\text{m}$ and $1.25 \mu\text{m}$ in 2MASS J0937+2931’s J -band spectrum (Burgasser et al. 2002a; K04), because low metallicity implies a paucity of sodium and because high gravity raises the abundance of KCl at the expense of K (Lodders 1999; Marley et al. 2002; K04). Recent models of the pressure-broadened Na I and K I absorption lines in the $0.6\text{--}1 \mu\text{m}$ spectrum of 2MASS J0937+2931 suggest that a mixed condition of high gravity and low metallicity best describe this unusual T dwarf (Burgasser et al. 2003a).

2MASS J0415–0935 (T9) is the latest T dwarf classified on the system of G02 (K04). It has been classified as type T8 by Burgasser et al. (2002a), but its numerical rank based on the average of its spectral indices is the latest of the T dwarfs in their sample. Our computed values of $\log(L_{\text{bol}}/L_{\odot}) = -5.73 \pm 0.05$ and $T_{\text{eff}} = 600\text{--}750$ K show that 2MASS J0415–0935 is

the least luminous and coolest brown dwarf presently known. It is 35–225 K cooler than the previous title-holder, Gl 570D (Burgasser et al. 2000; Geballe et al. 2001). Interestingly, the $J-H$ and $H-K$ colors of 2MASS J0415–0935 are redder than those of Gl 570D (K04), which is contrary to the trend that later T dwarfs have bluer colors in these bands. Marley et al. (2002) and Burrows, Sudarsky, & Lunine (2003) predict a reversal in $J-K$ as H_2O condenses and settles into clouds at $T_{\text{eff}} \lesssim 500$ K. If the redder JHK colors of 2MASS J0415–0935 are caused by thickening water clouds, then our computed value of T_{eff} indicates that the condensation of H_2O can occur under warmer conditions than anticipated from typical model atmospheres. However, Burrows, Sudarsky, & Lunine (2003) show that H_2O clouds can form at such temperatures in the atmospheres of very old ($\sim 6-10$ Gyr) brown dwarfs with masses $\sim 0.040-0.060 M_{\odot}$. Alternatively, the color reversal may be due to optically-thick clouds that conceivably form when gaseous potassium condenses into solid KCl at $T_{\text{eff}} \approx 600$ K (Lodders 1999; Marley 2000; Burrows, Sudarsky, & Lunine 2003). Further study of 2MASS J0415–0935 is needed to investigate these possibilities.

5. Effects of Precipitating Clouds, Nonequilibrium Chemistry, and Gravity

Our theoretical understanding of the effects of condensate clouds on the emergent fluxes of brown dwarfs has advanced considerably during the last few years (Burrows et al. 1997; Chabrier et al. 2000; Allard et al. 2001; Ackerman & Marley 2001; Marley et al. 2002; Burgasser et al. 2002b; Tsuji 2002; Tsuji & Nakajima 2003; Cooper et al. 2003; Burrows, Sudarsky, & Lunine 2003). The formation, migration, sedimentation, and turbulent disruption of cloud decks are thought to affect significantly the near-infrared spectra of L and T dwarfs, as well as cooler dwarfs yet to be discovered. The models of Ackerman & Marley (2001) and Marley et al. (2002) consider horizontally-uniform decks of precipitating water, iron, and silicate clouds formed in atmospheres having solar metallicity and conditions of structural and thermochemical equilibrium. The altitudes, particle-size distributions, and density profiles of the clouds are determined self-consistently from atmospheric temperature and pressure profiles and an adjustable ratio, f_{sed} , which describes the efficiency of particle sedimentation (precipitation) relative to the upward transport of condensates by convection.¹⁶ Practical values of f_{sed} for L dwarfs range from 3, which also describes Jupiter’s thick NH_3 cloud deck, to 5, which describes a thinner, more efficiently precipitating cloud deck (Ackerman & Marley 2001; Marley et al. 2002; Burgasser et al. 2002b; K04). Model spectra from 0.5 μm to 5.0 μm have been produced by Marley et al., and our L' and M' measurements allow us

¹⁶Ackerman & Marley (2001) originally employed the parameter f_{rain} to describe the sedimentation efficiency. To avoid confusion with the traditional notion of rain, f_{rain} has been renamed f_{sed} .

to assess these models between 3 μm and 5 μm .

Figures 8, 9, and 10 are diagrams of M_K , $M_{L'}$, and $M_{M'}$ versus T_{eff} for the L3–T9 dwarfs listed in Table 6. The dwarfs for which we have M' data are denoted by filled symbols to facilitate comparison of the data associated with these dwarfs in all three diagrams. The absolute magnitudes of close binaries have been increased by 0.75 mag to represent one component of the presumed uneclipsed, equal-luminosity systems. The curves in the diagrams are the predicted absolute magnitudes computed from the models of Marley et al. (2002) for discrete values of f_{sed} (3, 5, and no clouds) and surface gravity ($\log g = 4.5, 5.0, \text{ and } 5.5$, where g has units of cm s^{-2}). The precipitating-cloud models are shown for $2000 \geq T_{\text{eff}} \geq 1300$ K, and the cloud-free models are shown for $T_{\text{eff}} \leq 1500$ K. Thus, all models are shown across the L–T transition. The predicted magnitudes were synthesized from the model spectra and the measured transmission profiles of the MKO K , L' , and M' filters (L02). The diagrams show that the models collectively envelope the empirical data in all bands, i.e., the models reproduce the broad ranges of absolute magnitudes and effective temperatures for this sample of L and T dwarfs. The ensemble of data does not favor particular sets of model parameters for particular ranges of spectral type, but this situation is expected given the presumably heterogeneous masses, ages, and metallicities associated with our sample.

Figures 8–10 indicate that the high-gravity ($\log g = 5.0\text{--}5.5$) models consistently match the absolute magnitudes and effective temperatures obtained for the L3–T4.5 dwarfs in our sample. Conversely, the values of M_K and $M_{L'}$ for the T6–T9 dwarfs (except the anomalous 2MASS J0937+2931) are generally bounded by the low-gravity ($\log g = 4.5\text{--}5.0$) models. The lower gravities of the late-T dwarfs are also indicated in K04’s Figure 6, which compares the measured MKO $J\text{--}H$ and $H\text{--}K$ colors of 42 T dwarfs with those synthesized from the models of Marley et al. (2002). The apparent fidelity of the low-gravity models suggests that they are useful benchmarks for predicting other photometric characteristics of late-T dwarfs. Such reasoning has frequently been applied when estimating the fluxes of cool brown dwarfs at wavelengths longer than 4 μm , which are easily observed from space. Figure 10, however, shows that the values of $M'_{M'}$ measured for *all* the T dwarfs in our sample are better matched by the high-gravity models. The $\log g = 4.5\text{--}5.0$ models, which consistently reproduce M_K and $M'_{L'}$ measured for the late-T dwarfs Gl 229B and 2MASS J0415–0935, underestimate $M'_{M'}$ for these dwarfs by 0.5–1 mag. L02 also noted discrepancies of $\gtrsim 1$ mag between the measured $K\text{--}M'$ colors of two T dwarfs (SDSS J1254–0122 and 2MASS J0559–1404) and the $K\text{--}M'$ colors predicted by the dusty-atmosphere models of Chabrier et al. (2000) and the settled-condensate models of Burrows et al. (1997) for wide ranges of gravity. Noting that these models predicted M_K well for their sample of L and T dwarfs, L02 attributed the discrepancies to M' luminosities that were overpredicted by a factor of ~ 3 . This assessment

is consistent with the general trends seen in Figures 8–10, but the figures also show that 2MASS J0559–1404’s M_K , $M_{L'}$, and $M_{M'}$ are consistent with the cloud-free, $\log g = 5.5$ model of Marley et al. (2002).

Although the discrepancies between the observed and predicted M' luminosities of most T dwarfs vary among the models, they reveal a consistent overestimation of the emergent $5 \mu\text{m}$ flux regardless of how the condensates are modeled. L02 speculated that the low M' luminosities of SDSS J1254–0122 and 2MASS J0559–1404 are caused by strong CO absorption at 4.5–4.9 μm , which was predicted and then observed in the M -band spectrum of Gl 229B (Fegley & Lodders 1996; Noll, Geballe, & Marley 1997; Oppenheimer et al. 1998). The models of Burrows et al. (1997), Chabrier et al. (2000), and Marley et al. (2002) do not account for this absorption because it results from an abundance of CO that exceeds that expected under conditions of thermochemical equilibrium. Saumon et al. (2003) have modeled the effects of nonequilibrium chemistry caused by vertical mixing on the emergent spectrum of brown dwarfs. They determined that the overabundance of CO in cloudless atmospheres significantly decreases the M' fluxes from their chemical-equilibrium levels for $T_{\text{eff}} \lesssim 1400$ K. As Figure 6b shows, this range of T_{eff} spans the late half of the presently defined T sequence.¹⁷

Saumon et al. (2003) showed that the measured values of $M_{M'}$ for 2MASS J0559–1404 and Gl 229B are matched by a nonequilibrium model with $\log g = 5$ and an eddy-diffusion coefficient of $\sim 100 \text{ cm}^2 \text{ s}^{-1}$. Such a coefficient is consistent with the minimum expected for planetary atmospheres and indicates that the vertical mixing of CO occurs within the outermost radiative layer of the atmosphere. An independent measure of 2MASS J0559–1404’s gravity is needed, however, to resolve the ambiguity between the $\log g = 5$, nonequilibrium model of Saumon et al. (2003) and the cloud-free, $\log g = 5.5$, equilibrium model of Marley et al. (2002) shown in Figure 10. Our results for the T9 dwarf 2MASS J0415–0935 provide a less ambiguous test of the nonequilibrium models for the coolest known T dwarfs ($T_{\text{eff}} \approx 700$ K). Figures 8 and 10 show that the cloud-free, $\log g = 4.5$ model of Marley et al. (2002) matches M_K and $M_{L'}$ well, but it underestimates $M_{M'}$ by ~ 1 mag. Conversely, the $\log g = 5.5$ model predicts $M_{M'}$ within 0.25 mag, but overestimates M_K and $M_{L'}$ by 1.6 mag and 0.6 mag, respectively. Figure 4 of Saumon et al. (2003) shows that the measured $M_{M'} = 14.03 \pm 0.15$ for 2MASS J0415–0935 is well matched by a nonequilibrium, $\log g = 5$ model with a large

¹⁷Saumon et al. (2003) also predicted that nonequilibrium $\text{CO} \leftrightarrow \text{CH}_4$ chemistry should diminish the CH_4 absorption bands at 2.2–2.4 μm and 3.3–3.7 μm for late-L through mid-T dwarfs. The effect on the 2.2–2.4 μm band is convolved with the effects of a sinking and disrupting cloud deck over the L–T transition, but the 3.3–3.7 μm band suffers no such convolution. A comprehensive set of L -band spectra for late-L and mid-T dwarfs would therefore directly constrain the parameters of the nonequilibrium models.

eddy-diffusion coefficient ($\sim 10^4 \text{ cm}^2 \text{ s}^{-1}$) typical of planetary atmospheres.

Evolutionary models of ultracool dwarfs (Burrows et al. 1997; Chabrier et al. 2000) can be used to constrain the gravities and masses of the dwarfs in our sample, if the dwarfs’ ages can be estimated. D02 used kinematic statistics to argue that the mean age of the L and T dwarfs in the solar neighborhood is 2–4 Gyr. We find an age range of 0.3–5.5 Gyr for the dwarfs in our sample whose minimum and maximum ages can be constrained spectroscopically.¹³ The lower limit of this range is consistent with a reported lull in star formation in the solar neighborhood during the last ~ 0.5 Gyr (Hernandez, Valls-Gabaud, & Gilmore 2000; Gizis, Reid, & Hawley 2002). The evolutionary tracks of Burrows et al. (1997) show that L2–T4 dwarfs ($T_{\text{eff}} \approx 2000\text{--}1400$ K) with ages 0.3–5.5 Gyr have $\log g \approx 5.0\text{--}5.5$. This prediction is consistent with the results shown in Figures 8–10. The evolutionary tracks also show that T6–T9 dwarfs ($T_{\text{eff}} \approx 1000\text{--}700$ K) in this age range have $\log g \approx 4.5\text{--}5.3$, but their mean gravity is $\log g \gtrsim 5.0$ because high-mass brown dwarfs cool much more slowly than low-mass brown dwarfs (Reid et al. 1999). This range of gravity is higher than the $\log g \approx 4.5\text{--}5.0$ noted for T6–T9 dwarfs in Figures 8 and 9. Unfortunately, the small and heterogeneous nature of our sample precludes a definitive explanation of this discrepancy. Because the magnitudes of the late-T dwarfs are typically near the detection limits of 2MASS and SDSS, our sample may be biased toward younger, brighter, and less-massive ones. Alternatively, the gravities indicated by the solar-metallicity, equilibrium models of Marley et al. (2002) may be incorrect. Nevertheless, the latter possibility does not affect our conclusions regarding the overpredicted M' luminosities for late-T dwarfs.

6. Implications for Spaced-Based Missions

Burrows et al. (1997, 2001, 2003) created 1–30 μm spectra of brown dwarfs and extrasolar giant planets (EGPs) of various masses and ages using model atmospheres that assume settled condensate clouds and thermochemical equilibrium. They found that the suppression of mid-infrared flux by H_2 enhances enormously the flux at shorter wavelengths. For example, the 5 μm flux of a 1 Gyr-old, Jupiter-mass EGP is 10^4 times greater than its $T_{\text{eff}} \approx 160$ K blackbody equivalent. Marley et al. (1996) referred to this enhanced 5 μm flux as the “universal diagnostic” of brown dwarfs and EGPs. Burrows et al. (2001) remarked that space-based, M -band imagers could detect brown dwarfs cooler than can be found by DENIS, 2MASS, and SDSS. Burrows, Sudarsky, & Lunine (2003) added that the persistent M -band hump in the spectra of older and less massive brown dwarfs and EGPs makes this bandpass the best suited for studying these objects with the *Spitzer Space Telescope* (*SST*; formerly the *Space Infrared Telescope Facility*, or *SIRTF*). Such searches for “infra-T”

dwarfs and EGPs are indeed imminent now that *SST* has been launched (Padgett, O’Linger, & Stapelfeldt 2003; G. Fazio 2003, personal communication¹⁸).

The apparent 50–200% overestimates of the *M*-band fluxes of T dwarfs by chemical-equilibrium models diminish the anticipated sensitivity of the 4.5 μm band of *SST*’s Infrared Array Camera (IRAC) to the coolest known T dwarfs. If the especially low *M*’ luminosity of 2MASS J0415–0935 is indicative of low-mass brown dwarfs with $T_{\text{eff}} \lesssim 600$ K, then IRAC’s 4.5 μm detection horizons for nearby infra-T dwarfs and EGPs may be significantly nearer than expected. Moreover, the low-mass limits for members of young star clusters detected at 4.5 μm may be higher than anticipated. The 1.0 μm width of IRAC’s 4.5 μm bandpass will mitigate somewhat the effect of the 4.5–4.9 μm CO absorption on the integrated signal-to-noise ratio, but it will also complicate the interpretation of the CO absorption strength. By expanding our narrower-band *M*’ study to include more faint and cool brown dwarfs, we may aid the *SST* studies by calibrating the effects of CO absorption on the broader 4.5 μm photometry of at least the warmer IRAC targets.

Saumon et al. (2003) reported that nonequilibrium chemistry also affects the abundances of N_2 and NH_3 in the atmospheres of cool brown dwarfs. The observable effect of this situation is diminished absorption by NH_3 at 10.35 μm and 10.75 μm . Thus, contrary to the case of CO in the *M*-band, vertical mixing serves to enhance the *N*-band (~ 10 μm) flux of brown dwarfs with $T_{\text{eff}} \lesssim 1200$ K. Unfortunately, the *N*-band lies between the reddest bandpass of IRAC and the bluest bandpass of the Multiband Imaging Photometer for *SST* (MIPS), but targeted studies of extremely cool brown dwarfs with *SST*’s Infrared Spectrograph (IRS) should benefit from their larger-than-predicted 10 μm luminosities. Moreover, future mid-infrared space missions like the *James Webb Space Telescope (JWST)* may fully exploit the enhanced 10 μm luminosities of infra-T dwarfs and EGPs. Despite the previously underappreciated effects of nonequilibrium chemistry in substellar atmospheres, the prospects for filling the ever-shrinking gap between the coolest known T dwarfs and the Jovian planets with *SST* and *JWST* are excitingly good.

7. Summary

Our compilation of new and previously reported MKO *L*’ and *M*’ photometry has permitted us to characterize ultracool dwarfs comprehensively at wavelengths longward of the commonly used *J*, *H*, and *K* bands. We find that *K*–*L*’ increases monotonically with de-

¹⁸Presently, unpublished abstracts of the approved *SST* Guaranteed Time Observer science programs may be viewed on the World Wide Web at <http://sirtf.caltech.edu/SSC/geninfo/gto/abs/>.

creasing T_{eff} , but the nearly constant $T_{\text{eff}} \approx 1450$ K of spectral types L7–T4 limits the utility of $K-L'$ as an indicator of spectral type. Likewise, $L'-M'$ is nearly constant between types L6 and T3, indicating that the dramatic changes in the 1–2.5 μm spectra of L–T transition dwarfs are not duplicated in their L' - and M' -band spectra. This dichotomous behavior supports recent theories that the rapid migration, disruption, and/or thinning of condensate clouds at $T_{\text{eff}} \lesssim 1400$ K occur at altitudes that are coincident with the regions of z - through K -band emission but are well below the L' -band and M' -band “photospheres.” The L' and M' luminosities of the early-T dwarfs do not exhibit the pronounced humps or inflections noted by others in the I through K bands, but insufficient data exist for types L6–T5 to assert that $M_{L'}$ and $M_{M'}$ are strictly monotonic within this range of types.

We used our L' photometry, flux-calibrated JHK spectra, and recently published trigonometric parallaxes to compute L_{bol} , BC_K , and T_{eff} for ultracool dwarfs. We find that BC_K is a well behaved function of spectral type with a dispersion of ~ 0.1 mag for types M6–T5. BC_K is significantly more scattered among the later T dwarfs, which may indicate the sensitivity of H_2 CIA in the K -band to varying surface gravity for $T_{\text{eff}} \lesssim 1400$ K. BC_K is neither a monotonic nor single-valued function of $J-K$ because of the color reversal induced by the onset of CH_4 absorption at 2.2–2.4 μm at spectral type L8. BC_K is a single-valued function of $K-L'$ except at $K-L' \approx 1.6$, which corresponds to the L–T transition. T_{eff} declines steeply and monotonically for types M6–L7 and T4–T9, but is nearly constant at ~ 1450 K for types L7–T4 with assumed ages of ~ 3 Gyr. Our photometry and bolometric calculations indicate that Kelu-1 (L3) and SDSS J0423–0414 (T0) are probable binary systems. We compute $\log(L_{\text{bol}}/L_{\odot}) = -5.73 \pm 0.05$ and $T_{\text{eff}} = 600\text{--}750$ K for 2MASS J0415–0935 (T9), making it the least luminous and coolest brown dwarf presently known.

We have compared the measured absolute magnitudes of L3–T9 dwarfs with those predicted by the precipitating-cloud models of Marley et al. for varying surface gravities, g , and sedimentation efficiencies, f_{sed} . The models spanning $4.5 \leq \log g \leq 5.5$ and $f_{\text{sed}} = 3, 5$, and “ ∞ ” (no clouds) reproduce well the M_K and $M_{L'}$ of all the dwarfs in our sample. The models indicate that the L3–T4.5 dwarfs generally have higher gravities ($\log g = 5.0\text{--}5.5$) than the T6–T9 dwarfs ($\log g = 4.5\text{--}5.0$). The lower-gravity models underestimate $M_{M'}$ for the late-T dwarfs by 0.5–1 mag. This overestimation of the M' luminosity for $T_{\text{eff}} \lesssim 1000$ K is attributed to absorption at 4.5–4.9 μm by CO, which is not expected under the condition of thermochemical equilibrium assumed in the models. The impact of nonequilibrium chemistry on the broadband near-infrared fluxes of cool brown dwarfs has only recently been appreciated. Consequently, the effective-temperature limits of space-based 5 μm searches for infra-T dwarfs and EGPs, such as those planned with the recently-launched *Spitzer Space Telescope*, will be somewhat higher than originally expected.

The authors thank Didier Saumon for computing the model magnitudes shown in Figures 8–10. We also thank the referee, Neill Reid, for many helpful comments. We gratefully acknowledge the UKIRT staff for their assistance with the observations and data acquisition. Some data were obtained through the UKIRT Service Programme. DAG thanks the Center for Astrophysical Sciences at Johns Hopkins University for its moral and financial support of this work. MSM acknowledges support from NASA grants NAG2-6007 and NAG5-8919 and NSF grant AST 00-86288. UKIRT is operated by the Joint Astronomy Centre on behalf of the U. K. Particle Physics and Astronomy Research Council. Funding for the creation and distribution of the SDSS Archive has been provided by the Alfred P. Sloan Foundation, the Participating Institutions, the National Aeronautics and Space Administration, the National Science Foundation, the U. S. Department of Energy, the Japanese Monbukagakusho, and the Max Planck Society. The SDSS is managed by the Astrophysical Research Consortium for the Participating Institutions: The University of Chicago, Fermilab, the Institute for Advanced Study, the Japan Participation Group, The Johns Hopkins University, Los Alamos National Laboratory, the Max Planck Institute for Astronomy, the Max Planck Institute for Astrophysics, New Mexico State University, University of Pittsburgh, Princeton University, the United States Naval Observatory, and the University of Washington. The SDSS Web site is <http://www.sdss.org/>.

REFERENCES

- Ackerman, A. S., & Marley, M. S. 2001, *ApJ*, 556, 872
- Allard, F., Hauschildt, P. H., Alexander, D. R., Tamanai, A., Schweitzer, A. 2001, *ApJ*, 556, 357
- Baraffe, I., Chabrier, G., Allard, F., & Hauschildt, P. H. 1998, *A&A*, 337, 403
- Basri, G., Martín, E., Ruiz, M. T., Delfosse, X., Forveille, T., Epchtein, N., Allard, F., & Leggett, S. K. 1998, *ASP Conf. Ser.* 154, *The Tenth Cambridge Workshop on Cool Stars, Stellar Systems and the Sun*, eds. R. A. Donahue & J. A. Bookbinder (San Francisco: ASP), 1819
- Basri, G., Mohanty, S., Allard, F., Hauschildt, P. H., Delfosse, X., Martín, E. L., Forveille, T., & Goldman, B. 2000, *ApJ*, 538, 363
- Becklin, E. E., & Zuckerman, B. 1988, *Nature*, 336, 656
- Burgasser, A. J., Kirkpatrick, J. D., Brown, M. E., Reid, I. N., Burrows, A., Liebert, J., Matthews, K., Gizis, J. E., Dahn, C. C., Monet, D. G., Cutri, R. M., & Skrutskie, M. F. 2002a, *ApJ*, 564, 421
- Burgasser, A. J., Kirkpatrick, J. D., Cutri, R. M., McCallon, H., Kopan, G., Gizis, J. E., Liebert, J., Reid, I. N., Brown, M. E., Monet, D. G., Dahn, C. C., Beichman, C. A., & Skrutskie, M. F. 2000, *ApJ*, 531, L57
- Burgasser, A. J., Kirkpatrick, J. D., Liebert, J., & Burrows, A. 2003a, *ApJ*, 594, 510
- Burgasser, A. J., Kirkpatrick, J. D., McElwain, M. W., Cutri, R. M., Burgasser, A. J., & Skrutskie, M. F. 2003b, *AJ*, 125, 850
- Burgasser, A. J., Kirkpatrick, J. D., Reid, I. N., Brown, M. E., Miskay, C. L., & Gizis, J. E. 2003c, *ApJ*, 586, 512
- Burgasser, A. J., Marley, M. S., Ackerman, A. S., Saumon, D., Lodders, K., Dahn, C. C., Harris, H. C., & Kirkpatrick, J. D. 2002b, *ApJ*, 571, L151
- Burrows, A., Hubbard, W. B., Lunine, J. I., & Liebert, J. 2001, *Rev. Mod. Phys.*, 73, 719
- Burrows, A., Hubbard, W. B., Saumon, D., & Lunine, J. I. 1993, *ApJ*, 406, 158
- Burrows, A., Marley, M., Hubbard, W. B., Lunine, J. I., Guillot, T., Saumon, D., Freedman, R., Sudarsky, D., & Sharp, C. 1997, *ApJ*, 491, 856

- Burrows, A., & Sharp, C. M. 1999, ApJ, 512, 843
- Burrows, A., Sudarsky, D., & Lunine, J. I. 2003, ApJ, 596, 587
- Chabrier, G., Baraffe, I., Allard, F., & Hauschildt, P. 2000, ApJ, 542, 464
- Clarke, F. J., Tinney, C. G., & Covey, K. R. 2002, MNRAS, 332, 361
- Cooper, C. S., Sudarsky, D., Milsom, J. A., Lunine, J. I., & Burrows, A. 2003, ApJ, 586, 1320
- Cruz, K. L., Reid, I. N., Liebert, J., Kirkpatrick, J. D., & Lowrance, P. J. 2003, AJ, 126, 2421
- Dahn, C. C., Harris, H. C., Vrba, F. J., Guetter, H. H., Canzian, B., Henden, A. A., Levine, S. E., Luginbuhl, C. B., Monet, A. K. B., Monet, D. G., Pier, J. R., Stone, R. C., Walker, R. L., Burgasser, A. J., Gizis, J. E., Kirkpatrick, J. D., Liebert, J., & Reid, I. N. 2002, AJ, 124, 1170 (D02)
- Epchtein, N. 1997, in *The Impact of Large Scale Near-IR Sky Surveys*, eds. F. Garzón, N. Epchtein, A. Omont, W. B. Burton, and P. Persei (Dordrecht: Kluwer), 15
- ESA 1997, *The Hipparcos and Tycho Catalogues*, ESA SP-1200 (Noordwijk: ESA)
- Fegley, B., & Lodders, K. 1996, ApJ, 472, L37
- Freed, M., Close, L. M., & Siegler, N. 2003, ApJ, 584, 453
- Geballe, T. R., Knapp, G. R., Leggett, S. K., Fan, X., Golimowski, D. A., Anderson, S., Brinkmann, J., Csabai, I., Gunn, J. E., Hawley, S. L., Hennessy, G., Henry, T. J., Hill, G. J., Hindsley, R. B., Ivesić, Ž., Lupton, R. H., McDaniel, A., Munn, J. A., Narayanan, V. K., Peng, E., Pier, J. R., Rockosi, C. M., Schneider, D. P., Smith, J. A., Strauss, M. A., Tsvetanov, Z. I., Uomoto, A., York, D. G., & Zheng, W. 2002, ApJ, 564, 466 (G02)
- Geballe, T. R., Saumon, D., Leggett, S. K., Knapp, G. R., Marley, M. S., & Lodders, K. 2001, ApJ, 556, 373
- Gizis, J. E., Monet, D. G., Reid, I. N., Kirkpatrick, J. D., Liebert, J., & Williams, R. J. 2000, AJ, 120, 1085
- Gizis, J. E., Reid, I. N., & Hawley, S. L. 2002, AJ, 123, 3356

- Gliese, W., & Jahreiss, H. 1991, Preliminary Version of the Third Catalogue of Nearby Stars (Heidelberg: Astronomisches Rechen-Institut)
- Goldman, B., Delfosse, X., Forveille, T., Afonso, C., Alard, C., Albert, J. N., Andersen, J., Ansari, R., Aubourg, É., Bareyre, P., Bauer, F., Beaulieu, J. P., Borsenberger, J., Bouquet, A., Char, S., Charlot, X., Couchot, F., Coutures, C., Derue, F., Ferlet, R., Fouqué, P., Glicenstein, J. F., Gould, A., Graff, D., Gros, M., Haissinski, J., Hamilton, J. C., Hardin, D., de Kat, J., Kim, A., Lasserre, T., Lesquoy, É., Loup, C., Magneville, C., Mansoux, B., Marquette, J. B., Martín, E. L., Maurice, É., Milsztajn, A., Moniez, M., Palanque-Delabrouille, N., Perdureau, O., Prévot, L., Regnault, N., Rich, J., Spiro, M., Vidal-Madjar, A., Vigroux, L., & Zylberajch, S. 1999, *A&A*, 351, L5
- Griffith, C. A., & Yelle, R. V. 1999, *ApJ*, 519, L85
- Hawley, S. L., Covey, K. R., Knapp, G. R., Golimowski, D. A., Fan, X., Anderson, S. F., Gunn, J. E., Harris, H. C., Ivesić, Ž., Long, G. M., Lupton, R. H., McGehee, P. M., Narayanan, V., Peng, E., Schlegel, D., Schneider, D. P., Spahn, E. Y., Strauss, M. A., Szkody, P., Tsvetanov, Z., Walkowicz, L. M., Brinkmann, J., Harvanek, M., Hennessy, G. S., Kleinman, S. J., Krzesinski, J., Long, D., Neilsen, E. H., Newman, P. R., Nitta, A., Snedden, S. A., & York, D. G. 2002, *AJ*, 123, 3409
- Henry, T. J., Walkowicz, L. M., Barto, T. C., & Golimowski, D. A. 2002, *AJ*, 123, 2002
- Hernandez, X., Valls-Gabaud, D., & Gilmore, G. 2000, *MNRAS*, 316, 605
- Jones, H. R. A., Longmore, A. J., Allard, F., & Hauschildt, P. H. 1996, *MNRAS*, 280, 77
- Kirkpatrick, J. D., Allard, F., Bida, T., Zuckerman, B., Becklin, E. E., Chabrier, G., & Baraffe, I. 1999a, *ApJ*, 519, 834
- Kirkpatrick, J. D., Dahn, C. C., Monet, D. G., Reid, I. N., Gizis, J. E., Liebert, J., & Burgasser, A. J. 2001, *AJ*, 121, 3235
- Kirkpatrick, J. D., Henry, T. J., & McCarthy, D. W. 1991, *ApJS*, 77, 417
- Kirkpatrick, J. D., Reid, I. N., Liebert, J., Cutri, R. M., Nelson, B., Beichman, C. A., Dahn, C. C., Monet, D. G., Gizis, J. E., & Skrutskie, M. F. 1999b, *ApJ*, 519, 802
- Knapp, G. R., Leggett, S. K., Fan, X., Marley, M. S., Geballe, T. R., Golimowski, D. A., Finkbeiner, D., Gunn, J. E., Hennawi, J., Ivesić, Ž., Lupton, R. H., Schlegel, D. J., Strauss, M. A., Tsvetanov, Z. I., Chiu, K., Zheng, W., Vrba, F. J., Henden, A. A.,

- Luginbuhl, C. B., Guetter, H. H., Munn, J. A., Canzian, B., Schneider, D. P., & Brinkmann, J. 2004, *AJ*, in press (astro-ph/0402451) (K04)
- Koerner, D. W., Kirkpatrick, J. D., McElwain, M. W., & Bonaventura, N. R. 1999, *ApJ*, 526, L25
- Leggett, S. K., Allard, F., Geballe, T. R., Hauschildt, P. H. & Schweitzer, A. 2001, *ApJ*, 548, 908
- Leggett, S. K., Allard, F., & Hauschildt, P. H. 1998, *ApJ*, 509, 836
- Leggett, S. K., Golimowski, D. A., Fan, X., Geballe, T. R., Knapp, G. R., Brinkmann, J., Csabai, I., Gunn, J. E., Hawley, S. L., Henry, T. J., Hindsley, R., Ivesić, Ž, Lupton, R. H., Pier, J. R., Schneider, D. P., Smith, J. A., Strauss, M. A., Uomoto, A., & York, D. G. 2002a, *ApJ*, 564, 452 (L02)
- Leggett, S. K., Hauschildt, P. H., Allard, F., Geballe, T. R., & Baron, E. 2002b, *MNRAS*, 332, 78
- Leggett, S. K., Hawarden, T. G., Currie, M. J., Adamson, A. J., Carroll, T. C., Kerr, T. H., Kuhn, O. P., Seigar, M. S., Varricatt, W. P., & Wold, T. 2003, *MNRAS*, 345, 144
- Leggett, S. K., Toomey, D. W., Geballe, T. R., & Brown, R. H. 1999, *ApJ*, 517, L139
- Lodders, K. 1999, *ApJ*, 519, 793
- Marley, M. 2000, *ASP Conf. Ser.* 212, *From Giant Planets to Cool Stars*, eds. C. A. Griffith & M. S. Marley (San Francisco: ASP), 152
- Marley, M. S., Saumon, D., Guillot, T., Freedman, R. S., Hubbard, W. B., Burrows, A., & Lunine, J. I. 1996, *Science*, 272, 1919
- Marley, M. S., Seager, S., Saumon, D., Lodders, K., Ackerman, A. S., Freedman, R. S., & Fan, X. 2002, *ApJ*, 568, 335
- Martín, E. L., Brandner, W. & Basri, G. 1999a, *Science*, 283, 1718
- Martín, E. L., Delfosse, X., Basri, G., Goldman, B., Forveille, T., & Zapatero Osorio, M. R. 1999b, *AJ*, 118, 2466
- Matthews, K., Nakajima, T., Kulkarni, S. R., & Oppenheimer, B. R. 1996, *AJ*, 112, 1678
- Nakajima, T., Oppenheimer, B. R., Kulkarni, S. R., Golimowski, D. A., Matthews, K., & Durrance, S. T. 1995, *Nature*, 378, 463

- Noll, K. S., Geballe, T. R., Leggett, S. K., & Marley, M. S. 2000, *ApJ*, 541, L75
- Noll, K. S., Geballe, T. R., & Marley, M. S. 1997, *ApJ*, 489, L87
- Oppenheimer, B. R., Kulkarni, S. R., Matthews, K., & van Kerkwijk, M. H. 1998, *ApJ*, 502, 932
- Padgett, D., O’Linger, J., & Stapelfeldt, K. 2003, in *IAU Symp. 211, Brown Dwarfs*, ed. E. Martín (San Francisco: ASP), 515
- Puxley, P. J., Sylvester, J., Pickup, D. A., Paterson, M. J., Laird, D. C., & Atad-Ettedgui, E. I. 1994, *Proc. SPIE*, 2198, 350
- Ramsay-Howat, S. K., Ellis, M. A., Gostick, D. C., Hastings, P. R., Strachan, M., & Wells, M. 2000, *Proc. SPIE*, 4008, 1067
- Reid, I. N., & Cruz, K. L. 2002, *AJ*, 123, 466
- Reid, I. N., Gizis, J. E., Kirkpatrick, J. D., & Koerner, D. W. 2001, *AJ*, 121, 489
- Reid, I. N., Kirkpatrick, J. D., Liebert, J., Burrows, A., Gizis, J. E., Burgasser, A., Dahn, C. C., Monet, D., Cutri, R., Beichman, C. A., & Skrutskie, M. 1999, *ApJ*, 521, 613
- Ruiz, M. T., Leggett, S. K., & Allard, F. 1997, *ApJ*, 491, L107
- Saumon, D., Bergeron, P., Lunine, J. I., Hubbard, W. B., & Burrows, A. 1994, *ApJ*, 424, 333
- Saumon, D., Geballe, T. R., Leggett, S. K., Marley, M. S., Freedman, R. S., Lodders, K., Fegley, B., & Sengupta, S. K. 2000, *ApJ*, 541, 374
- Saumon, D., Marley, M. S., Lodders, K., & Freedman, R. S. 2003, in *IAU Symp. 211, Brown Dwarfs*, ed. E. Martín (San Francisco: ASP), 345
- Schweitzer, A., Gizis, J. E., Hauschildt, P. H., Allard, F., Howard, E. M., & Kirkpatrick, J. D. 2002, *ApJ*, 566, 435
- Simons, D. A., & Tokunaga A. T. 2002, *PASP*, 114, 169
- Skrutskie, M. F., et al. 1997, in *The Impact of Large Scale Near-IR Sky Surveys*, eds. F. Garzón, N. Epchtein, A. Omont, W. B. Burton, and P. Persei (Dordrecht: Kluwer), 25
- Stephens, D. C. 2003, in *IAU Symp. 211, Brown Dwarfs*, ed. E. Martín (San Francisco: ASP), 355

- Stephens, D. C., & Leggett, S. K. 2004, *PASP*, 116, 9
- Stephens, D. C., Marley, M. S., Noll, K. S., & Chanover, N. 2001, *ApJ*, 556, L97
- Tinney, C. G. 1996, *MNRAS*, 281, 644
- Tinney, C. G., Burgasser, A. J., & Kirkpatrick, J. D. 2003, *AJ*, 126, 975
- Tinney, C. G., Reid, I. N., Gizis, J., & Mould, J. R. 1995, *AJ*, 110, 3014
- Tokunaga, A. T., & Kobayashi, N. 1999, *AJ*, 117, 1010
- Tokunaga, A. T., Simons, D. A., & Vacca, W. D. 2002, *PASP*, 114, 180
- Tsuji, T. 2002, *ApJ*, 575, 264
- Tsuji, T., & Nakajima, T. 2003, *ApJ*, 585, L151
- Tsuji, T., & Ohnaka, K. 1995, in *Elementary Processes in Dense Plasmas*, eds. S. Ichimaru and S. Ogata (Reading: Addison-Wesley), 193
- Tsuji, T., Ohnaka, K., & Aoki, W. 1995, in *The Bottom of the Main Sequence and Beyond*, ed. C. G. Tinney (Berlin: Springer), 45
- van Altena, W. F., Lee, J. T., & Hoffleit, E. D. 1995, *The General Catalogue of Trigonometric Stellar Parallaxes* (4th ed.; New Haven: Yale Univ. Obs.)
- Vrba, F. J., Henden, A. A., Luginbuhl, C. B., Guetter, H. H., Munn, J. A., Canzian, B., Burgasser, A. J., Kirkpatrick, J. D., Fan, X., Geballe, T. R., Golimowski, D. A., Knapp, G. R., Leggett, S. K., Schneider, D. P., & Brinkmann, J. 2004, *AJ*, in press (astro-ph/0402272) (V04)
- York, D. G., et al. 2000, *AJ*, 120, 1579

Table 1. The Sample

Name ^a	Spectral Type	π (error) ^b (mas)	$M - m$ (error) ^b	References ^c		
				SpT	π	Mult.
Gl 229A	M1	173.17 (1.10)	1.192 (0.014)	1	2,3	4
LHS 102A	M3.5	104.7 (11.4)	0.100 (0.236)	5	3	6
LHS 315	M4	298.72 (1.35)	2.376 (0.010)	7	2,3	...
LHS 11	M4.5	224.8 (2.9)	1.759 (0.028)	1	3	...
LHS 333AB	M5.5 + M7	227.9 (4.6)	1.789 (0.044)	8	3	8
LHS 36	M6	419.1 (2.1)	3.112 (0.011)	9	3	...
LHS 292	M6.5	220.3 (3.6)	1.715 (0.035)	9	3	...
LHS 3003	M7	156.3 (3.0)	0.970 (0.042)	9	3	...
LP 326–21 ^d	M8	10
LP 349–25 ^e	M8	10
LHS 2397aAB	M8 + L7.5	68.65 (1.87)	–0.817 (0.059)	8	3,11	12
TVLM 513–46546	M8.5	94.5 (0.6)	–0.123 (0.014)	9 ^f	13,14	...
LHS 2065	M9	117.3 (1.5)	0.346 (0.028)	9 ^g	3	...
LHS 2924	M9	92.4 (1.3)	–0.172 (0.031)	1	3	...
BRI 0021–0214	M9.5	84.2 (2.6)	–0.373 (0.067)	9 ^h	3,13	...
2MASS J03454316+2540233	L1	37.1 (0.5)	–2.153 (0.029)	9	14	...
2MASS J14392836+1929149	L1	69.6 (0.5)	–0.787 (0.016)	15	14	...
2MASS J07464256+2000321AB	L1 + \sim L2	81.9 (0.3)	–0.434 (0.008)	9	14	16
DENIS-P J1058.7–1548	L3	57.7 (1.0)	–1.194 (0.038)	9	14	...
GD 165B	L3	31.7 (2.5)	–2.495 (0.171)	9	3	17
Kelu-1	L3	53.6 (2.0)	–1.354 (0.081)	9	14	...
2MASS J22244381–0158521	L3.5	87.02 (0.89)	–0.302 (0.022)	15	14,18	...
2MASS J00361617+1821104	L4	114.2 (0.8)	0.288 (0.015)	9	14	...
LHS 102B	L4.5	104.7 (11.4)	0.100 (0.236)	19	3	6
SDSS J053951.99–005902.0	L5	76.12 (2.17)	–0.593 (0.062)	9	18	...
SDSS J224953.47+004404.6	L5	9
2MASS J15074769–1627386	L5.5	136.4 (0.6)	0.674 (0.010)	15	14	...
SDSS J010752.33+004156.1	L5.5	64.13 (4.51)	–0.965 (0.153)	9	18	...
DENIS-P J0205.4–1159AB	L5.5 + L5.5	50.6 (1.5)	–1.479 (0.064)	9	14	20
2MASS J08251968+2115521	L6	94.22 (0.88)	–0.129 (0.020)	9	14,18	...
DENIS-P J1228.2–1547AB	L6 + \sim L6	49.4 (1.9)	–1.531 (0.084)	9	14	21
2MASS J08503593+1057156AB	L6 + \sim L8.5	33.84 (2.69)	–2.353 (0.173)	22	14,18	18
2MASS J16322911+1904407	L7.5	65.02 (1.77)	–0.935 (0.059)	9	14	...
2MASS J22443167+2043433	L7.5	15
Gl 584C ⁱ	L8	54.37 (1.14)	–1.323 (0.046)	9	2,3,18	23
SDSS J003259.36+141036.6	L8	30.14 (5.16)	–2.604 (0.372)	9	18	...
SDSS J085758.45+570851.4	L8	9
2MASS J03105986+1648155	L9	9
2MASS J09083803+5032088	L9 ^j	15
SDSS J080531.80+481233.0	L9	15
SDSS J083008.12+482847.4	L9	76.42 (3.43)	–0.584 (0.097)	9	18	...
2MASS J03284265+2302051	L9.5	33.13 (4.20)	–2.399 (0.275)	9	18	...
SDSS J204749.61–071818.3	L9.5	15
SDSS J042348.57–041403.5	T0	65.93 (1.70)	–0.905 (0.056)	9	18	...
SDSS J120747.17+024424.8	T0	15
SDSS J015141.69+124429.6	T1	46.73 (3.37)	–1.652 (0.157)	9	18	...
SDSS J075840.33+324723.4	T2	15
SDSS J125453.90–012247.4	T2	73.96 (1.59)	–0.655 (0.047)	9	18,24	...

Table 1—Continued

Name ^a	Spectral Type	π (error) ^b (mas)	$M - m$ (error) ^b	References ^c		
				SpT	π	Mult.
SDSS J102109.69–030420.1	T3	35.35 (4.24)	–2.258 (0.260)	9	18,24	...
2MASS J2254188+312349	T4	15
2MASS J05591914–1404488	T4.5	96.73 (0.96)	–0.072 (0.022)	9	14,18	...
2MASS J15031961+2525196	T5.5	25
2MASS J15344984–2952274AB	T5.5 + T5.5	73.6 (1.2)	–0.666 (0.035)	26	24	27
Gl 229B	T6	173.17 (1.10)	1.192 (0.014)	9	2,3	4
2MASS J0243137–245329	T6	93.62 (3.63)	–0.143 (0.084)	26	18	...
2MASS J09373487+2931409	T6 ^k	162.84 (3.88)	1.059 (0.052)	15	18	...
SDSS J123147.39+084730.7	T6	15
SDSS J162414.37+002915.6	T6	90.73 (1.03)	–0.211 (0.025)	9	14,18,24	...
2MASS J12255432–2739466AB	T6 + T8	74.79 (2.03)	–0.631 (0.059)	9	18,24	27
Gl 570D ^l	T8	170.16 (1.45)	1.154 (0.019)	9	2,3	28
2MASS J0727182+171001	T8	110.14 (2.34)	0.210 (0.046)	15	18	...
2MASS J12171110–0311131	T8	93.20 (2.06)	–0.153 (0.048)	9	18,24	...
2MASS J0415195–093506	T9	174.34 (2.76)	1.207 (0.034)	15

^aIAU approved designations for 2MASS and SDSS point sources are “2MASS Jhhmmss[.]ss±ddmss[.]s” and “SDSS Jhhmmss.ss±ddmss.s,” where the equatorial coordinates are given at equinox J2000. Preliminary designations are given for 2MASS sources whose IAU-approved designations are unpublished.

^bBased on weighted mean of referenced trigonometric parallaxes.

^cReferences for principal spectral type, trigonometric parallax, and multiplicity: (1) Kirkpatrick, Henry, & McCarthy 1991, (2) ESA 1997, (3) van Altena, Lee, & Hoffleit 1995, (4) Nakajima et al. 1995, (5) Martín et al. 1999b, (6) Goldman et al. 1999, (7) Henry et al. 2002, (8) Gliese & Jahreiss 1991, (9) G02, (10) Gizis et al. 2000, (11) Tinney 1996, (12) Freed, Close, & Siegler 2003, (13) Tinney et al. 1995, (14) Dahn et al. 2002, (15) Knapp et al. 2004, (16) Reid et al. 2001, (17) Becklin & Zuckerman 1988, (18) Vrba et al. 2004, (19) Leggett et al. 2002b, (20) Koerner et al. 1999, (21) Martín, Brandner, & Basri 1999a, (22) Kirkpatrick et al. 1999b, (23) Kirkpatrick et al. 2001, (24) Tinney, Burgasser, & Kirkpatrick 2003, (25) Burgasser et al. 2003b, (26) Classified on scheme of G02 using spectra of Burgasser et al. 2002a, (27) Burgasser et al. 2003c (28) Burgasser et al. 2000

^dAlso known as 2MASSW J1444171+300214.

^eAlso known as 2MASSW J0027559+221932.

^fName abbreviated to T 513 by G02.

^gMisidentified as “LHS 2025” by G02.

^hName abbreviated to BRI 0021 by G02.

ⁱAlso known as 2MASS J15232263+3014562.

^jClassified as L5 by Cruz et al. (2003) from optical spectrum.

^kLabelled “peculiar” by Burgasser et al. (2002a) because of low K -band flux.

^lAlso known as 2MASSW J1457150–212148.

Table 2. New MKO L' and M' Photometry

Name	L' (error)	Imager	Date	M' (error)	Imager	Date
SDSS J0032+1410	13.35 (0.05)	UIST	2003 Sep 04
SDSS J0151+1244	13.54 (0.05)	IRCAM	2001 Nov 25
DENIS J0205–1159AB	12.10 (0.20)	IRCAM	2001 Nov 23
2MASS J0243–2453	13.25 (0.05)	IRCAM	2001 Nov 24
2MASS J0328+2302	13.33 (0.05)	UIST	2003 Nov 08
2MASS J0415–0935	13.28 (0.05)	IRCAM	2001 Nov 25	12.82 (0.15)	IRCAM	2001 Nov 25
SDSS J0423–0414	11.90 (0.05)	UIST	2003 Jan 04
SDSS J0539–0059	11.87 (0.10)	UIST	2003 Jan 04
2MASS J0727+1710	13.68 (0.05)	IRCAM	2001 Nov 25
SDSS J0758+3247	11.94 (0.03)	UIST	2003 Jan 04
SDSS J0758+3247	12.06 (0.05)	UIST	2003 Nov 10
SDSS J0805+4812	12.31 (0.05)	UIST	2003 Nov 10
2MASS J0908+5032	11.37 (0.06)	IRCAM	2002 Jun 18	11.95 (0.20)	UIST	2002 Dec 06
2MASS J0937+2931	12.34 (0.05)	IRCAM	2001 Nov 24	11.74 (0.10)	IRCAM	2001 Nov 25
Gl 229A	4.04 (0.05)	IRCAM	2001 Nov 23
Gl 229B	12.24 (0.05)	IRCAM	2001 Nov 23	11.74 (0.10)	IRCAM	2001 Nov 23
SDSS J1021–0304	13.64 (0.05)	IRCAM	2001 Nov 23
SDSS J1207+0244	12.62 (0.05)	UIST	2003 May 16
SDSS J1231+0847	13.52 (0.05)	UIST	2003 May 16
Kelu-1	11.22 (0.10)	IRCAM	2002 Jun 21
2MASS J1439+1929	11.13 (0.06)	IRCAM	2002 Jun 18
2MASS J1503+2525	11.91 (0.05)	UIST	2003 Jan 04	12.25 (0.15)	UIST	2003 May 16
2MASS J1507–1627	10.69 (0.05)	IRCAM	2002 Jun 18
2MASS J1534–2952AB	12.58 (0.05)	UIST	2003 May 17
SDSS J2047–0718	13.80 (0.05)	IRCAM	2001 Nov 25
2MASS J2224–0158	10.90 (0.05)	IRCAM	2002 Jul 15	11.32 (0.05)	UIST	2003 Jun 04
2MASS J2244+2043	12.11 (0.03)	UIST	2003 Jan 04
SDSS J2249+0044	12.71 (0.07)	UIST	2003 Jun 18
2MASS J2254+3123	13.24 (0.05)	IRCAM	2001 Nov 24

Table 3. MKO $KL'M'$ Photometry of M, L, and T Dwarfs

Name	Spectral Type	$M_{L'}$ (error) ^a	L' (error)	$K-L'$ (error)	$L'-M'$ (error)
Gl 229A ^b	M1	5.25 (0.05)	4.06 (0.05)	0.09 (0.07)	0.02 (0.07)
LHS 102A ^c	M3.5	7.63 (0.24)	7.53 (0.05)	0.20 (0.06)	...
LHS 315	M4	7.62 (0.01)	5.24 (0.01)	0.41 (0.04)	...
LHS 11	M4.5	8.08 (0.08)	6.32 (0.07)	0.33 (0.08)	...
LHS 333AB	M5.5 + M7	7.42 (0.07)	5.63 (0.05)	0.45 (0.06)	...
LHS 36 ^d	M6	8.82 (0.05)	5.71 (0.05)	0.35 (0.06)	-0.14 (0.06)
LHS 292 ^d	M6.5	9.16 (0.06)	7.45 (0.05)	0.50 (0.06)	-0.20 (0.07)
LHS 3003	M7	9.40 (0.05)	8.43 (0.03)	0.50 (0.05)	...
LP 326-21 ^e	M8	...	10.09 (0.07)	...	-0.30 (0.12)
LP 349-25 ^e	M8	...	9.15 (0.07)	...	-0.24 (0.12)
LHS 2397aAB	M8 + L7.5	9.21 (0.06)	10.03 (0.02)	0.66 (0.04)	...
TVLM 513-46546	M8.5	9.92 (0.08)	10.04 (0.08)	0.65 (0.09)	...
LHS 2065 ^{e,f}	M9	9.74 (0.08)	9.39 (0.07)	0.52 (0.05)	-0.23 (0.10)
LHS 2924	M9	9.95 (0.04)	10.12 (0.03)	0.60 (0.05)	...
BRI 0021-0214	M9.5	9.41 (0.15)	9.78 (0.13)	0.75 (0.14)	...
2MASS J0345+2540	L1	9.86 (0.10)	12.01 (0.10)	0.65 (0.11)	...
2MASS J1439+1929	L1	10.01 (0.05)	10.80 (0.05)	0.67 (0.06)	-0.33 (0.08)
2MASS J0746+2000AB ^d	L1 + ~L2	9.24 (0.03)	9.67 (0.03)	0.76 (0.04)	-0.35 (0.08)
DENIS J1058-1548	L3	10.43 (0.11)	11.62 (0.10)	0.93 (0.11)	...
GD 165B	L3	10.43 (0.18)	12.93 (0.07)	1.16 (0.08)	...
Kelu-1	L3	9.43 (0.17)	10.78 (0.15)	1.00 (0.16)	-0.44 (0.18)
2MASS J2224-0158 ^g	L3.5	10.60 (0.05)	10.90 (0.05)	1.08 (0.06)	-0.42 (0.07)
2MASS J0036+1821	L4	10.37 (0.05)	10.08 (0.05)	0.96 (0.06)	-0.27 (0.07)
LHS 102B ^c	L4.5	10.51 (0.24)	10.41 (0.05)	0.95 (0.06)	...
SDSS J0539-0059	L5	10.73 (0.08)	11.32 (0.05)	1.08 (0.06)	-0.55 (0.11)
SDSS J2249+00	L5	...	12.71 (0.07)	1.69 (0.08)	...
2MASS J1507-1627	L5.5	10.65 (0.03)	9.98 (0.03)	1.31 (0.04)	-0.71 (0.06)
SDSS J0107+0041	L5.5	11.10 (0.17)	12.06 (0.07)	1.52 (0.08)	...
DENIS J0205-1159AB	L5.5 + L5.5	9.96 (0.12)	11.44 (0.10)	1.55 (0.10)	-0.66 (0.22)
2MASS J0825+2115	L6	11.40 (0.04)	11.53 (0.03)	1.40 (0.04)	...
DENIS J1228-1547AB	L6 + ~L6	9.89 (0.13)	11.42 (0.10)	1.29 (0.11)	...
2MASS J0850+1057AB	L6 + ~L8.5	10.59 (0.18)	12.94 (0.05)	1.41 (0.06)	...
2MASS J1632+1904	L7.5	11.60 (0.08)	12.54 (0.05)	1.43 (0.07)	...
2MASS J2244+2043 ^g	L7.5	...	12.11 (0.03)	1.79 (0.04)	...
Gl 584C	L8	11.54 (0.07)	12.86 (0.05)	1.49 (0.07)	...
SDSS J0032+1410	L8	10.75 (0.38)	13.35 (0.05)	1.64 (0.07)	...
SDSS J0857+5708	L8	...	11.31 (0.05)	1.63 (0.06)	-0.19 (0.11)
2MASS J0310+1648	L9	...	12.54 (0.05)	1.64 (0.06)	...

Table 3—Continued

Name	Spectral Type	$M_{L'}$ (error) ^a	L' (error)	$K-L'$ (error)	$L'-M'$ (error)
2MASS J0908+5032 ^g	L9	...	11.37 (0.06)	1.52 (0.07)	-0.58 (0.21)
SDSS J0805+4812	L9	...	12.31 (0.05)	1.20 (0.06)	...
SDSS J0830+4828	L9	11.40 (0.11)	11.98 (0.05)	1.70 (0.06)	...
2MASS J0328+2302	L9.5	10.93 (0.28)	13.33 (0.05)	1.54 (0.06)	...
SDSS J2047-0718 ^g	L9.5	...	13.80 (0.05)	1.54 (0.06)	...
SDSS J0423-0414	T0	10.55 (0.08)	11.45 (0.05)	1.51 (0.06)	-0.45 (0.07)
SDSS J1207+0244 ^g	T0	...	12.62 (0.05)	1.54 (0.06)	...
SDSS J0151+1244	T1	11.89 (0.16)	13.54 (0.05)	1.64 (0.07)	...
SDSS J0758+3247 ^{g,h}	T2	...	11.97 (0.03)	1.90 (0.04)	...
SDSS J1254-0122	T2	11.60 (0.07)	12.25 (0.05)	1.59 (0.06)	-0.40 (0.21)
SDSS J1021-0304	T3	11.38 (0.26)	13.64 (0.05)	1.62 (0.07)	...
2MASS J2254+3123 ^g	T4	...	13.24 (0.05)	1.79 (0.06)	...
2MASS J0559-1404	T4.5	12.07 (0.05)	12.14 (0.05)	1.59 (0.06)	-0.01 (0.16)
2MASS J1503+2525 ^g	T5.5	...	11.91 (0.05)	2.08 (0.06)	-0.34 (0.16)
2MASS J1534-2952AB ^g	T5.5 + T5.5	11.91 (0.06)	12.58 (0.05)	2.33 (0.06)	...
Gl 229B	T6	13.43 (0.05)	12.24 (0.05)	2.12 (0.06)	0.50 (0.11)
2MASS J0243-2453 ^g	T6	13.11 (0.10)	13.25 (0.05)	2.09 (0.06)	...
2MASS J0937+2931 ^g	T6	13.40 (0.07)	12.34 (0.05)	3.05 (0.08)	0.60 (0.11)
SDSS J1231+0847 ^g	T6	...	13.52 (0.05)	1.94 (0.06)	...
SDSS J1624+0029	T6	13.39 (0.05)	13.60 (0.04)	2.01 (0.06)	...
2MASS J1225-2739AB	T6 + T8	12.59 (0.10)	13.22 (0.08)	2.06 (0.09)	...
Gl 570D	T8	14.13 (0.05)	12.98 (0.05)	2.54 (0.07)	...
2MASS J0727+1710 ^g	T8	13.89 (0.07)	13.68 (0.05)	2.01 (0.06)	...
2MASS J1217-0311	T8	13.81 (0.07)	13.96 (0.05)	1.96 (0.06)	...
2MASS J0415-0935 ^g	T9	14.49 (0.06)	13.28 (0.05)	2.55 (0.06)	0.46 (0.16)

^aBased on weighted mean trigonometric parallaxes. See Table 1.

^b L' from Leggett et al. (2002b).

^c KL' from Leggett et al. (2002b).

^d M' from Reid & Cruz (2002).

^e $L'M'$ from Reid & Cruz (2002).

^f K synthesized from spectra of G02.

^g K from Knapp et al. (2004).

^h L' is weighted mean of values listed in Table 2.

Table 4. Polynomial Fits to Diagrams

$P(x)^a$	x	RMS ^b	Polynomial coefficients						
			c_0	c_1	c_2	c_3	c_4	c_5	c_6
M_K	$0.09 \leq K-L' \leq 2.55$	0.49	4.0760e+00	1.9467e+01	-2.1584e+01	1.1235e+01	-1.9583e+00
M_K	$0.21 \leq K-M' \leq 3.01$	0.43	8.2327e+00	6.9722e+00	-3.3255e+00	6.5907e-01
$M_{L'}$	$M1 \leq \text{SpT}^c \leq T9$	0.35	4.3095e+00	1.1450e+00	-8.0385e-02	2.4832e-03	-2.2539e-05
$M_{M'}$	$M1 \leq \text{SpT}^c \leq T9$	0.45	3.5211e+00	1.1826e+00	-6.4508e-02	1.2549e-03
BC_K	$M6 \leq \text{SpT}^c \leq T9$	0.13	3.9257e+00	-3.8338e-01	5.3597e-02	-2.6550e-03	4.0859e-05
T_{eff}	$M6 \leq \text{SpT}^c \leq T9$	124 K	1.4322e+04	-5.1287e+03	9.0951e+02	-8.3099e+01	4.0323e+00	-9.8598e-02	9.5373e-04

$$^a P(x) = \sum_{i=0}^n c_i x^i$$

^bUnits are magnitudes except where noted.

^cFit requires numerical translation of spectral types: M1–M9.5 → 1–9.5, L0–L9.5 → 10–19.5, T0–T9 → 20–29.

Table 5. Supplemental Dwarfs Lacking $L'M'$ Measurements

Name ^a	Spectral Type	π (error) ^b (mas)	$M - m$ (error) ^b	Measured M_K (error)	Estimated ^c $M_{L'}$ (error)	References ^d		
						SpT	π	K
SDSS J225529.09-003433.4	M8.5	16.19 (2.59)	-3.954 (0.347)	10.33 (0.35)	9.68 (0.36)	1	2	3
SDSS J144600.60+002452.0	L5	45.46 (3.25)	-1.712 (0.155)	12.09 (0.16)	10.83 (0.23)	1	2	3
SDSS J132629.82-003831.5	L5.5	49.98 (6.33)	-1.506 (0.275)	12.66 (0.28)	11.25 (0.32)	1	2	4
SDSS J083717.21-000018.0	T0.5	33.70 (13.45)	-2.362 (0.867)	13.62 (0.87)	12.04 (0.88)	1	2	3
SDSS J175032.96+175903.9	T3.5	36.24 (4.53)	-2.204 (0.271)	13.82 (0.28)	12.11 (0.32)	1	2	3
SDSS J020742.83+000056.2	T4.5	34.85 (9.87)	-2.289 (0.615)	14.33 (0.62)	12.54 (0.64)	1	2	3
2MASSI J2356547-155310	T6	68.97 (3.42)	-0.807 (0.108)	14.92 (0.11)	12.98 (0.19)	5	2	4
SDSS J134646.45-003150.4	T6	69.07 (2.09)	-0.804 (0.066)	14.93 (0.08)	12.87 (0.18)	1	2,6	3
2MASSI J1047538+212423	T6.5	98.75 (3.30)	-0.027 (0.073)	16.17 (0.08)	13.67 (0.18)	1	2,6	3

^aNaming protocol as described in Table 1.

^bBased on weighted mean of referenced trigonometric parallaxes.

^c L' estimated from dwarfs in Table 1 with similar spectral types and JHK colors. Errors include dispersions from fits to $K-L'$ versus spectral type (§4.1) of 0.06 mag (M dwarfs), 0.15 mag (L dwarfs), and 0.16 mag (T dwarfs).

^dReferences for spectral type, trigonometric parallax, and K photometry: (1) G02, (2) V04, (3) L02, (4) K04, (5) Classified on scheme of G02 using spectra of Burgasser et al. 2002a, (6) Tinney, Burgasser, & Kirkpatrick 2003

Table 6. Bolometric Luminosity and Effective Temperature

Name	Spectral Type	M_{bol} (error)	BC_K (error)	$\log(L_{\text{bol}}/L_{\odot})$ (error)	T_{eff} (K)	
					Range ^a	3 Gyr ^b
Gl 229A ^c	M1	7.97 (0.09)	2.63 (0.07)	−1.29 (0.02)	3750–3775	3755
LHS 102A ^c	M3.5	10.55 (0.25)	2.72 (0.06)	−2.32 (0.10)	3200–3300	3275
LHS 36	M6	12.18 (0.08)	3.01 (0.07)	−2.97 (0.02)	2650–2900	2900
LHS 292	M6.5	12.65 (0.09)	2.98 (0.07)	−3.16 (0.03)	2475–2750	2725
LHS 3003	M7	12.95 (0.09)	3.05 (0.07)	−3.28 (0.03)	2350–2650	2600
SDSS J2255–0034 ^d	M8.5	13.51 (0.36)	3.18 (0.07)	−3.50 (0.14)	2000–2525	2400
TVLM 513–46546	M8.5	13.73 (0.08)	3.16 (0.07)	−3.59 (0.02)	2025–2325	2300
LHS 2065	M9	13.47 (0.09)	3.21 (0.07)	−3.49 (0.02)	2150–2425	2400
BRI 0021–0214	M9.5	13.37 (0.10)	3.21 (0.07)	−3.45 (0.03)	2150–2475	2425
2MASS J0345+2540	L1	13.75 (0.08)	3.24 (0.07)	−3.60 (0.02)	2000–2325	2300
2MASS J1439+1929	L1	13.88 (0.07)	3.20 (0.06)	−3.66 (0.02)	1950–2275	2250
2MASS J0746+2000AB	L1 + \sim L2	13.26 (0.07)	3.26 (0.06)	−3.41 (0.02)	1900–2225 ^e	2200 ^e
DENIS J1058–1548	L3	14.73 (0.09)	3.37 (0.07)	−4.00 (0.03)	1600–1950	1900
GD 165B	L3	14.90 (0.19)	3.31 (0.07)	−4.06 (0.07)	1750–1925	1850
Kelu-1	L3	13.74 (0.11)	3.31 (0.07)	−3.59 (0.04)	2100–2350	2300 ^f
2MASS J2224–0158	L3.5	15.14 (0.07)	3.46 (0.06)	−4.15 (0.02)	1475–1800	1750
2MASS J0036+1821	L4	14.67 (0.07)	3.34 (0.06)	−3.97 (0.02)	1650–1975	1900
LHS 102B ^c	L4.5	14.89 (0.25)	3.43 (0.06)	−4.05 (0.10)	1750–1975	1850
SDSS J0539–0059	L5	15.12 (0.09)	3.31 (0.06)	−4.15 (0.03)	1475–1800	1750
SDSS J1446+0024 ^d	L5	15.43 (0.18)	3.34 (0.07)	−4.27 (0.07)	1300–1725	1650
2MASS J1507–1627	L5.5	15.16 (0.07)	3.20 (0.06)	−4.16 (0.02)	1475–1800	1750
SDSS J0107+0041	L5.5	15.93 (0.17)	3.32 (0.06)	−4.47 (0.06)	1175–1550	1475
SDSS J1326–0038 ^d	L5.5	15.94 (0.28)	3.28 (0.06)	−4.48 (0.11)	1150–1600	1475
DENIS J0205–1159AB	L5.5 + L5.5	14.71 (0.09)	3.20 (0.06)	−3.98 (0.03)	1350–1700 ^e	1650 ^e
2MASS J0825+2115	L6	16.10 (0.07)	3.30 (0.06)	−4.54 (0.02)	1175–1475	1425
DENIS J1228–1547AB	L6 + L6	14.50 (0.11)	3.32 (0.07)	−3.90 (0.04)	1400–1775 ^e	1700 ^e
2MASS J1632+1904	L7.5	16.23 (0.11)	3.19 (0.07)	−4.59 (0.03)	1150–1450	1375
Gl 584C	L8	16.20 (0.11)	3.17 (0.09)	−4.58 (0.04)	1300–1400	1350 ^f
SDSS J0032+1410 ^d	L8	15.46 (0.39)	3.07 (0.09)	−4.28 (0.15)	1250–1800	1650
SDSS J0830+4828	L9	16.19 (0.13)	3.09 (0.08)	−4.58 (0.05)	1125–1475	1400
2MASS J0328+2302 ^d	L9.5	15.53 (0.29)	3.06 (0.08)	−4.31 (0.11)	1250–1750	1625
SDSS J0423–0414	T0	15.11 (0.10)	3.05 (0.08)	−4.14 (0.04)	1450–1825	1750
SDSS J0837–0000 ^d	T0.5	16.50 (0.87)	2.88 (0.09)	−4.70 (0.35)	900–1600	1300
SDSS J0151+1244	T1	16.46 (0.19)	2.93 (0.09)	−4.68 (0.07)	1050–1425	1300
SDSS J1254–0122	T2	16.08 (0.10)	2.90 (0.08)	−4.54 (0.04)	1150–1500	1425
SDSS J1021–0304	T3	15.76 (0.28)	2.76 (0.09)	−4.40 (0.11)	1200–1650	1525
SDSS J1750+1759 ^d	T3.5	16.35 (0.29)	2.53 (0.09)	−4.64 (0.11)	1050–1475	1350
2MASS J0559–1404	T4.5	16.07 (0.13)	2.41 (0.13)	−4.53 (0.05)	1150–1500	1425
SDSS J0207+0000 ^d	T4.5	16.80 (0.63)	2.47 (0.13)	−4.82 (0.25)	875–1450	1200
2MASS J0243–2453	T6	17.45 (0.15)	2.25 (0.13)	−5.08 (0.06)	825–1150	1025
2MASS J0937+2931	T6	17.96 (0.16)	1.51 (0.14) ^g	−5.28 (0.05)	725–1000	900
2MASS J2356–1553 ^d	T6	17.26 (0.17)	2.34 (0.13)	−5.00 (0.06)	875–1200	1075
Gl 229B ^c	T6	17.77 (0.08)	2.22 (0.07)	−5.21 (0.02)	850–1050	950
SDSS J1346–0031 ^d	T6	17.25 (0.15)	2.32 (0.13)	−5.00 (0.06)	875–1200	1075
SDSS J1624+0029	T6	17.64 (0.14)	2.24 (0.13)	−5.16 (0.05)	800–1100	975
2MASS J1225–2739AB	T6 + T8	16.86 (0.14)	2.21 (0.13)	−4.85 (0.05)	800–1100 ^e	975 ^e
2MASS J1047+2124	T6.5	18.13 (0.15)	1.96 (0.13)	−5.35 (0.06)	725–950	900
2MASS J0727+1710	T8	18.14 (0.14)	2.24 (0.13)	−5.35 (0.05)	725–950	900

Table 6—Continued

Name	Spectral Type	M_{bol} (error)	BC_K (error)	$\log(L_{\text{bol}}/L_{\odot})$ (error)	T_{eff} (K)	
					Range ^a	3 Gyr ^b
2MASS J1217–0311	T8	18.05 (0.14)	2.28 (0.13)	–5.32 (0.05)	725–975	900
Gl 570D	T8	18.57 (0.14)	1.90 (0.13)	–5.53 (0.05) ^h	784–824 ^h	800
2MASS J0415–0935	T9	19.07 (0.13)	2.03 (0.13)	–5.73 (0.05)	600–750	700

^aRange of T_{eff} for assumed ages of 0.1–10 Gyr and known parallax uncertainties. The ages of Gl 229AB, LHS 102AB, GD 165B, Gl 584C, Gl 570D, and Kelu-1 have been further constrained observationally (see footnote 13).

^b T_{eff} at age ~ 3 Gyr, unless otherwise noted.

^c M_{bol} , BC_K and $\log(L_{\text{bol}}/L_{\odot})$ from Leggett et al. (2002b).

^d L' estimated from spectral type and JHK colors (§4.3).

^eAssuming uneclipsed components of equal luminosity.

^f T_{eff} given for middle of age range given in footnote 13.

^gStrongly depressed K -band flux produces atypical BC_K .

^h $\log(L_{\text{bol}}/L_{\odot})$ and T_{eff} from Geballe et al. (2001).

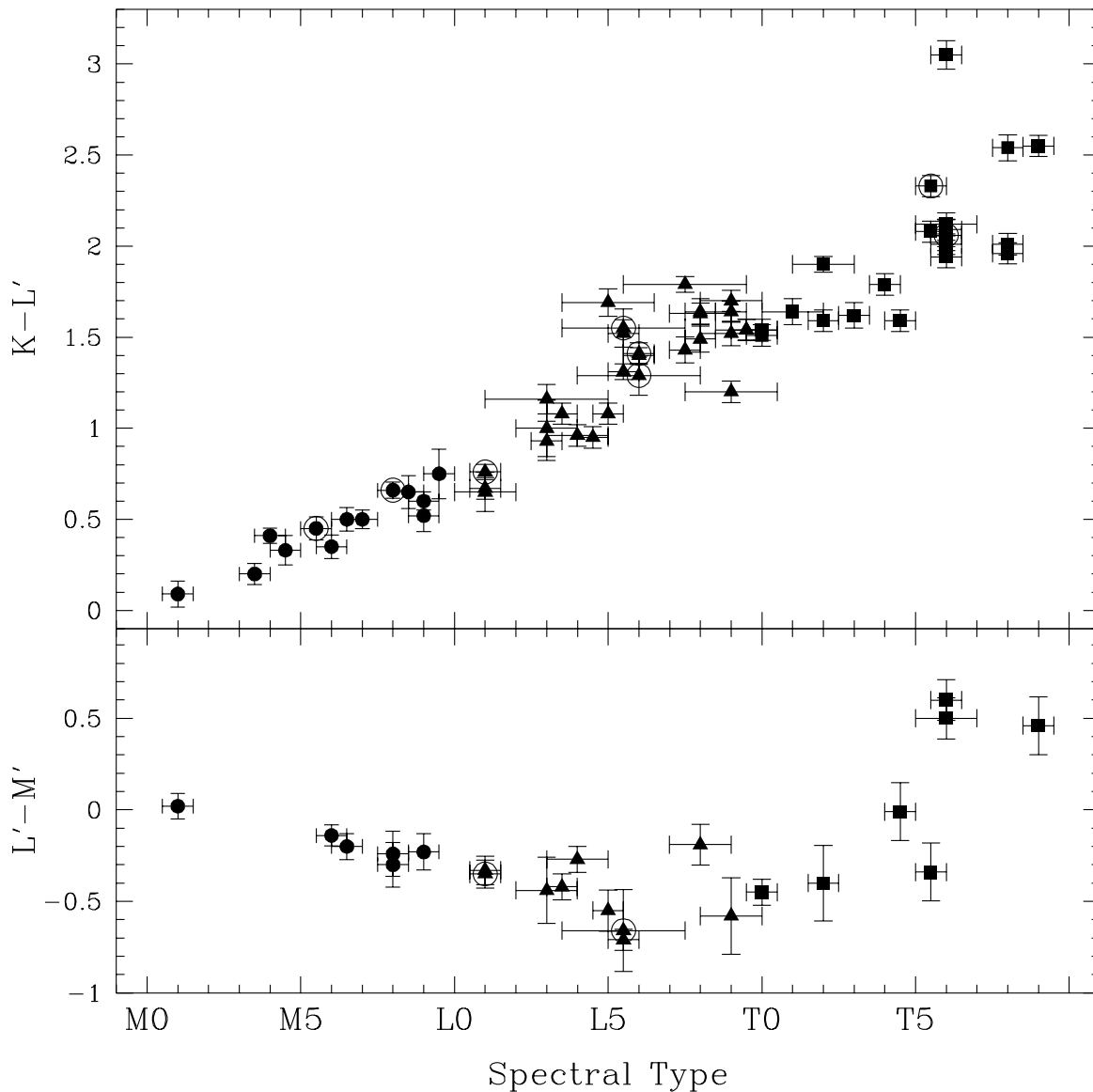


Fig. 1.— Variations of $K-L'$ and $L'-M'$ with spectral type for M dwarfs (circles), L dwarfs (triangles), and T dwarfs (squares) listed in Table 3. All data are based on the MKO photometric system. Points representing close-binary systems are surrounded by open circles. The L9 dwarf with the anomalously blue $K-L' = 1.20$ is SDSS J0805+4812, and the T6 dwarf with the anomalously red $K-L' = 3.05$ is 2MASS J0937+2931. Both dwarfs are discussed in §4.5.

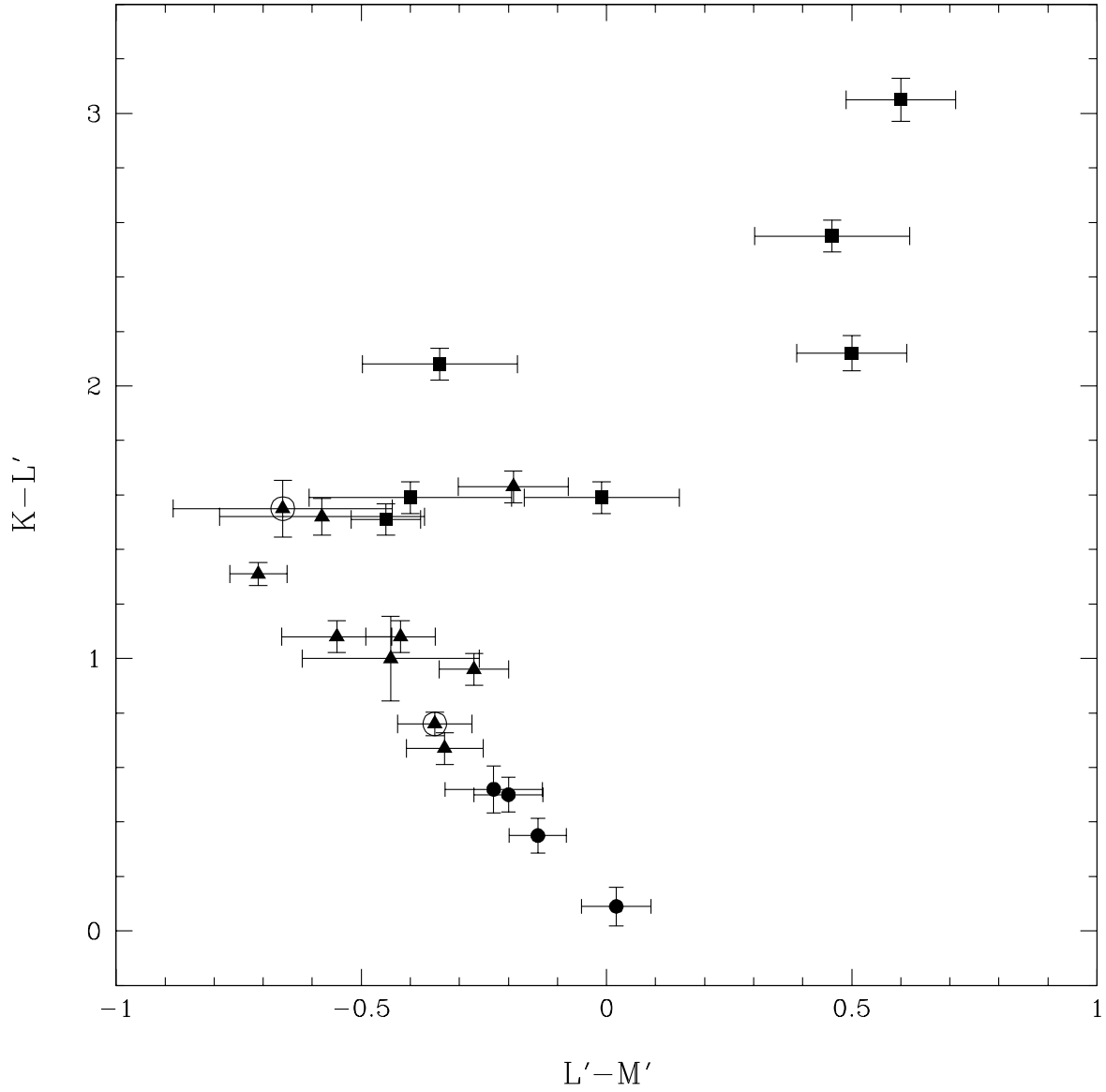


Fig. 2.— Color-color diagram of $K-L'$ versus $L'-M'$ for M, L, and T dwarfs listed in Table 3. All data are based on the MKO photometric system. All symbols are described in Figure 1.

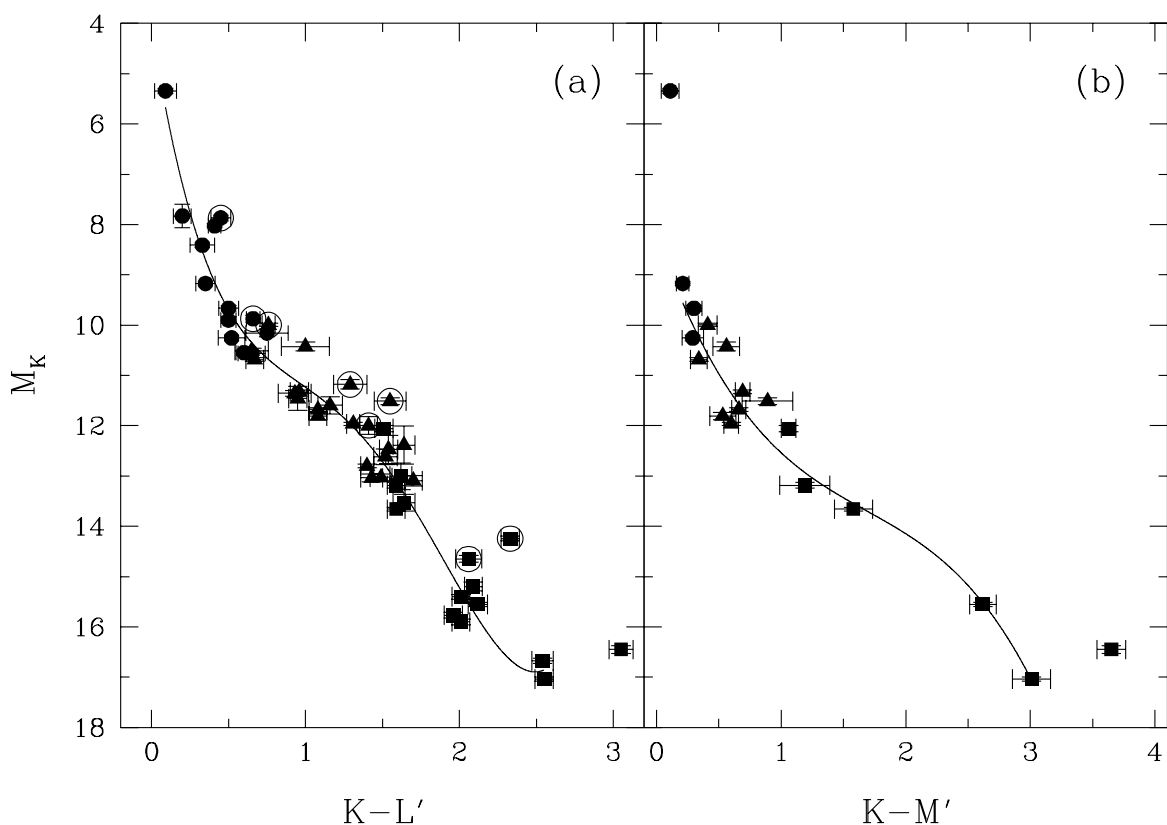


Fig. 3.— Color-magnitude diagrams of (a) M_K versus $K-L'$ and (b) M_K versus $K-M'$ for M, L, and T dwarfs listed in Table 3. All data are based on the MKO photometric system. All symbols are described in Figure 1. The M_K extrema represent Gl 229A (M1) and 2MASS J0415–0935 (T9). The curves are (a) fourth-order and (b) third-order polynomial fits to the unweighted data except those representing known close-binary systems (encircled points) and the anomalously red 2MASS J0937+2931 ($K-L' = 3.05$, $K-M' = 3.65$). The datum for Gl 229A ($K-M' = 0.11$) was also omitted from the fit in (b).

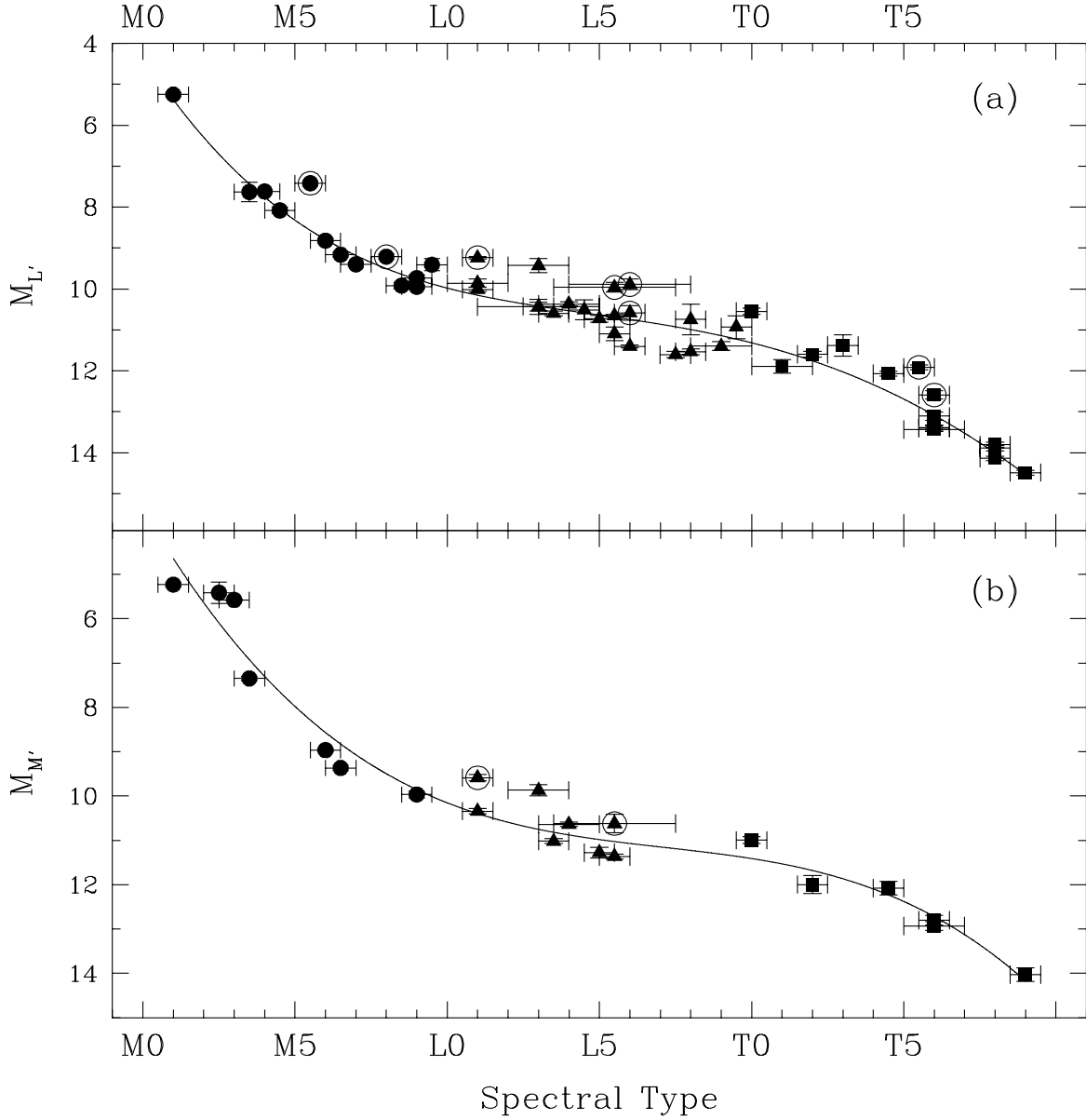


Fig. 4.— Diagrams of (a) M_L and (b) $M_{M'}$ versus spectral type for M, L, and T dwarfs listed in Table 3. All data are based on the MKO photometric system. All symbols are described in Figure 1. Diagram (b) is supplemented with MKO M' measurements reported by Reid & Cruz (2002) for Gl 811.1 (M2.5; G02), Gl 752A (M3; Kirkpatrick, Henry, & McCarthy 1991), and Gl 643 (M3.5; G02). The weighted means of the parallaxes of these M dwarfs measured by Yale Observatory (van Altena, Lee, & Hoffleit 1995) and *Hipparcos* (ESA 1997) are, respectively, 55.81 ± 6.27 mas, 171.01 ± 0.62 mas, and 158.28 ± 3.45 mas. The curves are (a) fourth-order and (b) third-order polynomial fits to the unweighted data except those representing known close-binary systems (encircled points).

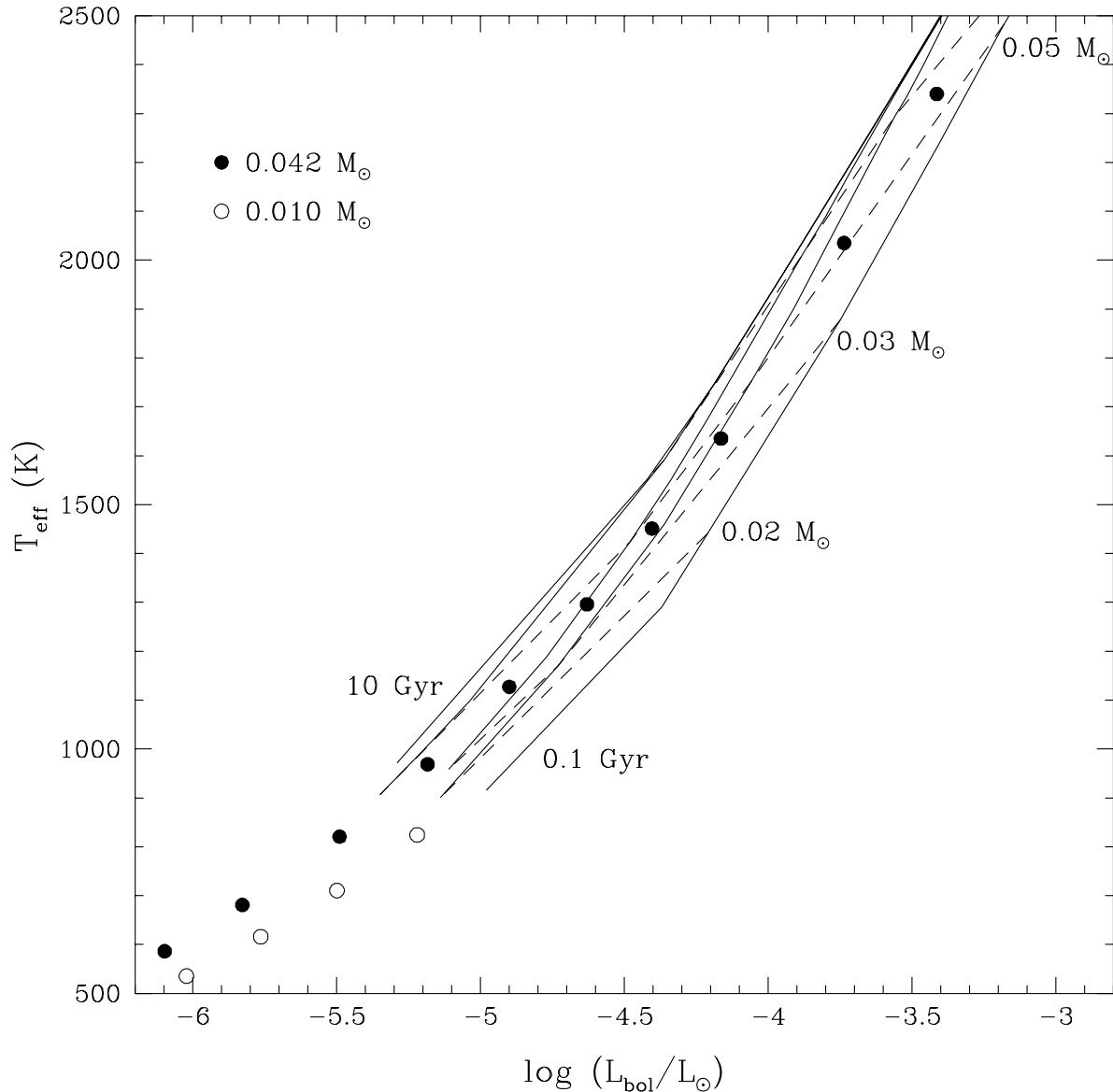


Fig. 5.— Predicted evolutions of L_{bol} and T_{eff} as functions of mass and age. The diagram is an extension to lower T_{eff} of Figure 12 of Leggett et al. (2001). The solid curves are, from right to left, the 0.1, 0.5, 1, 5, and 10 Gyr isochrones for 0.01–0.08 M_{\odot} brown dwarfs computed from the DUSTY atmosphere models of Chabrier et al. (2000). The dashed curves are, from top to bottom, the cooling tracks for 0.07, 0.05, 0.03, and 0.02 M_{\odot} brown dwarfs computed from the same models. Also shown are the cooling tracks for 0.042 M_{\odot} (filled circles) and 0.010 M_{\odot} (open circles) brown dwarfs of ages 0.1–10 Gyr and 0.1–0.5 Gyr, respectively, computed from the settled-dust models of Burrows et al. (1997) for time intervals of ~ 0.2 dex. Despite the differences between the two models’ treatment of photospheric condensates, the predicted cooling tracks from each model are mutually consistent. The range of T_{eff} for fixed L_{bol} never exceeds ~ 300 K.

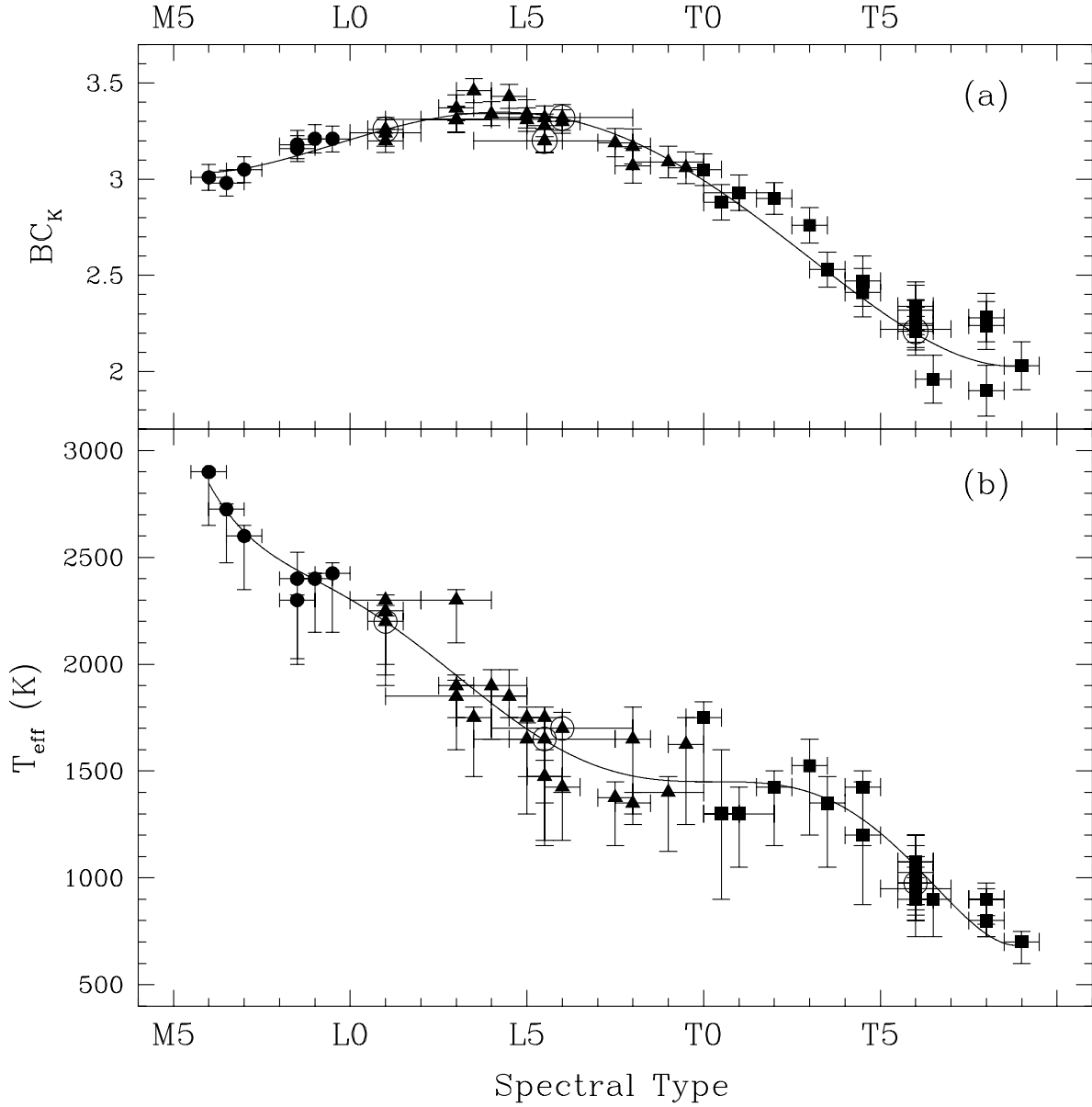


Fig. 6.— Diagrams of (a) BC_K and (b) T_{eff} versus spectral type for ultracool dwarfs listed in Table 6. All symbols are described in Figure 1. The plotted values of T_{eff} are those listed in Column 7 of Table 6 for a mean age of 3 Gyr, unless otherwise noted. The error bars for these values reflect the full ranges of T_{eff} listed in Column 6 of Table 6. The curves are (a) fourth-order and (b) sixth-order polynomial fits to the weighted data except those representing known close-binary systems (encircled points). The datum for the T6 dwarf 2MASS J0937+2931 ($BC_K = 1.51$) is not shown in (a), but it is included in the polynomial fit. The fit in (b) is fixed at type T9 to avoid an unrealistic upturn in T_{eff} between types T8 and T9.

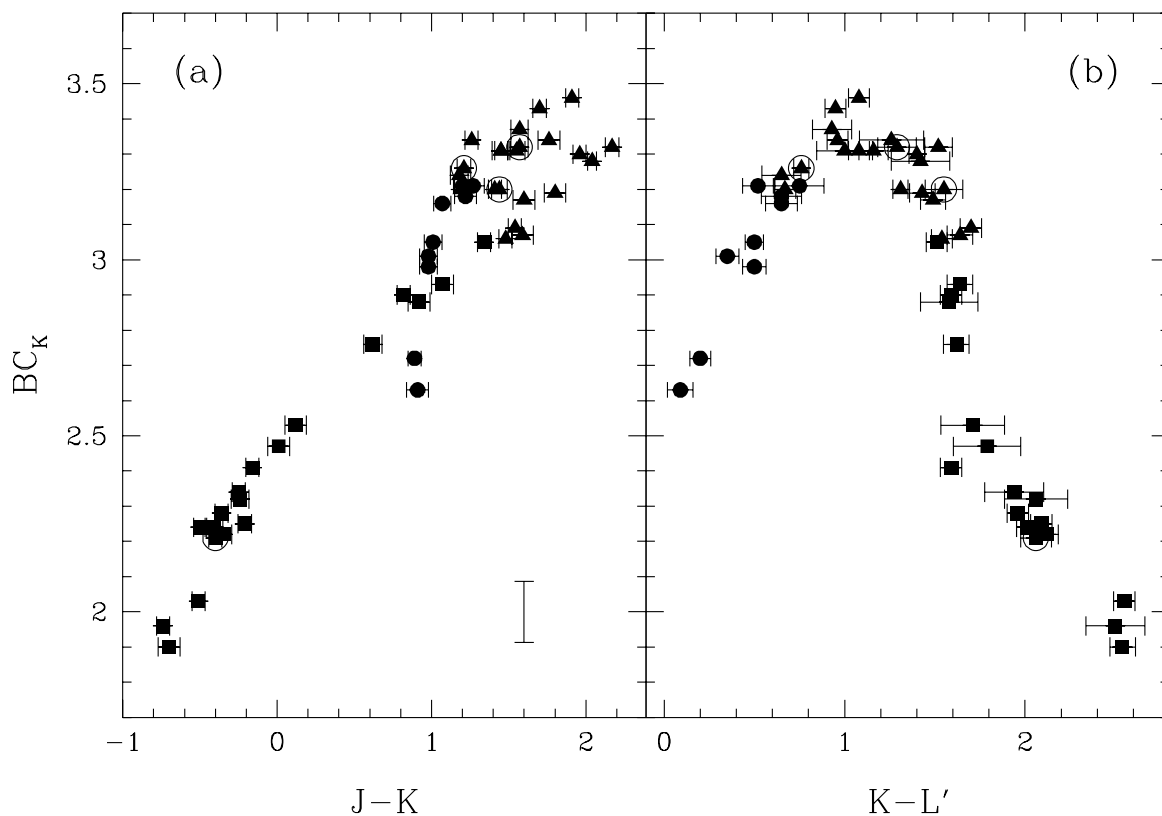


Fig. 7.— Diagrams of BC_K versus (a) $J-K$ and (b) $K-L'$ for dwarfs listed in Table 6. All data are based on the MKO photometric system; J measurements are taken from L02 and K04. All symbols are described in Figure 1. The uncertainty in BC_K for each point is omitted for clarity; the average uncertainty is represented by the vertical error bar in the lower right corner of (a). The data for the T6 dwarf 2MASS J0937+2931 ($BC_K = 1.51$) are not shown.

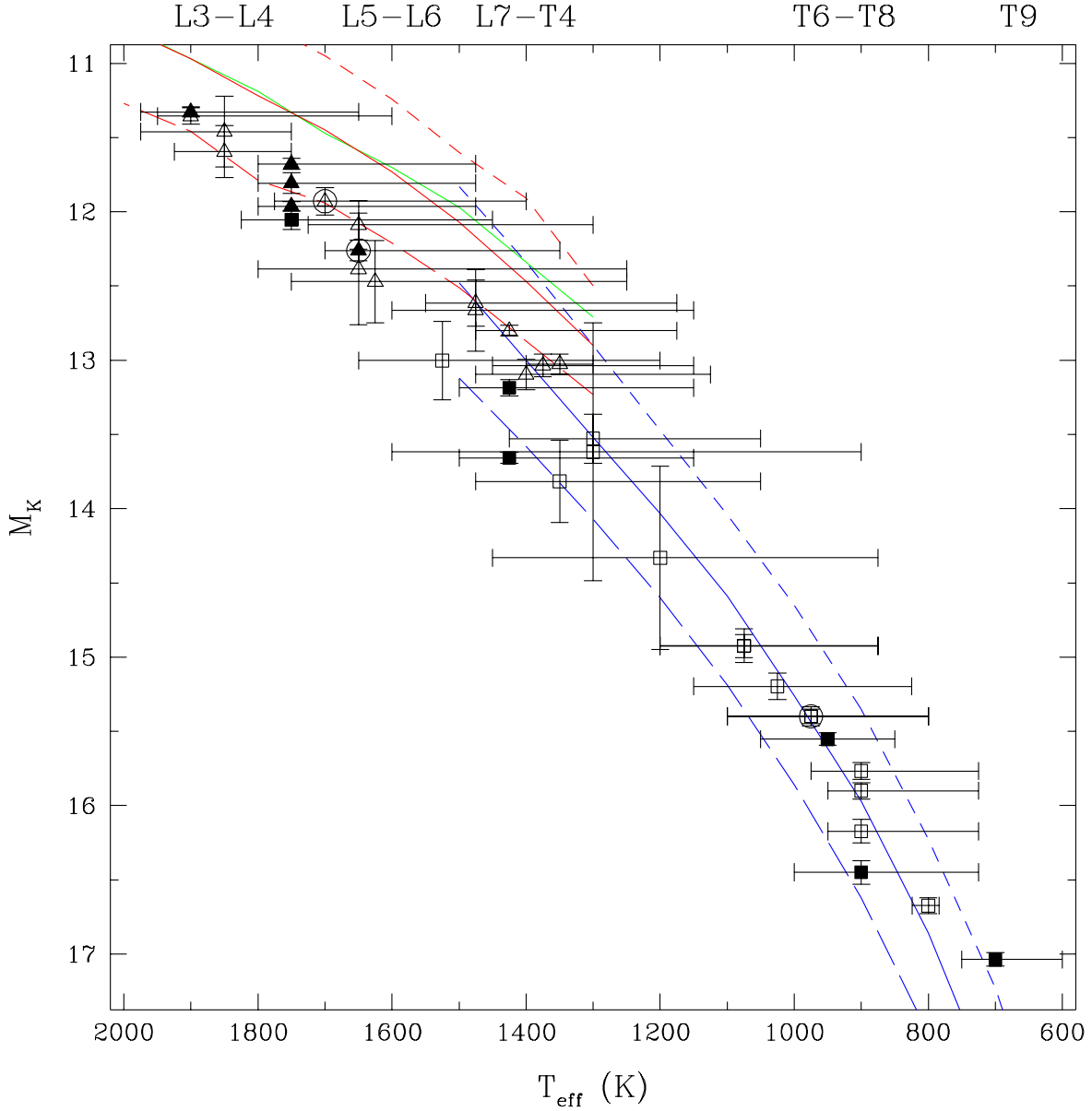


Fig. 8.— Diagram of M_K versus T_{eff} for L3–T9 dwarfs listed in Table 6. The plotted values of T_{eff} are those listed in Column 7 of Table 6 for a mean age of ~ 3 Gyr, unless otherwise noted. The error bars for these values reflect the full ranges of T_{eff} listed in Column 6 of Table 6. L dwarfs are represented by triangles and T dwarfs are represented by squares. Filled symbols denote those dwarfs for which we have M' photometric data (Figure 10). The measured values of M_K for close binaries (encircled points) have been increased by 0.75 mag to represent one component of the presumed unclipped, equal-luminosity systems. The curves are the predicted relationships from the models of Marley et al. (2002) for brown dwarfs with $f_{\text{sed}} = 3$ (green), $f_{\text{sed}} = 5$ (red), and cloud-free atmospheres (blue), and surface gravities of $\log g = 4.5$ (short-dash), 5.0 (solid), and 5.5 (long-dash).

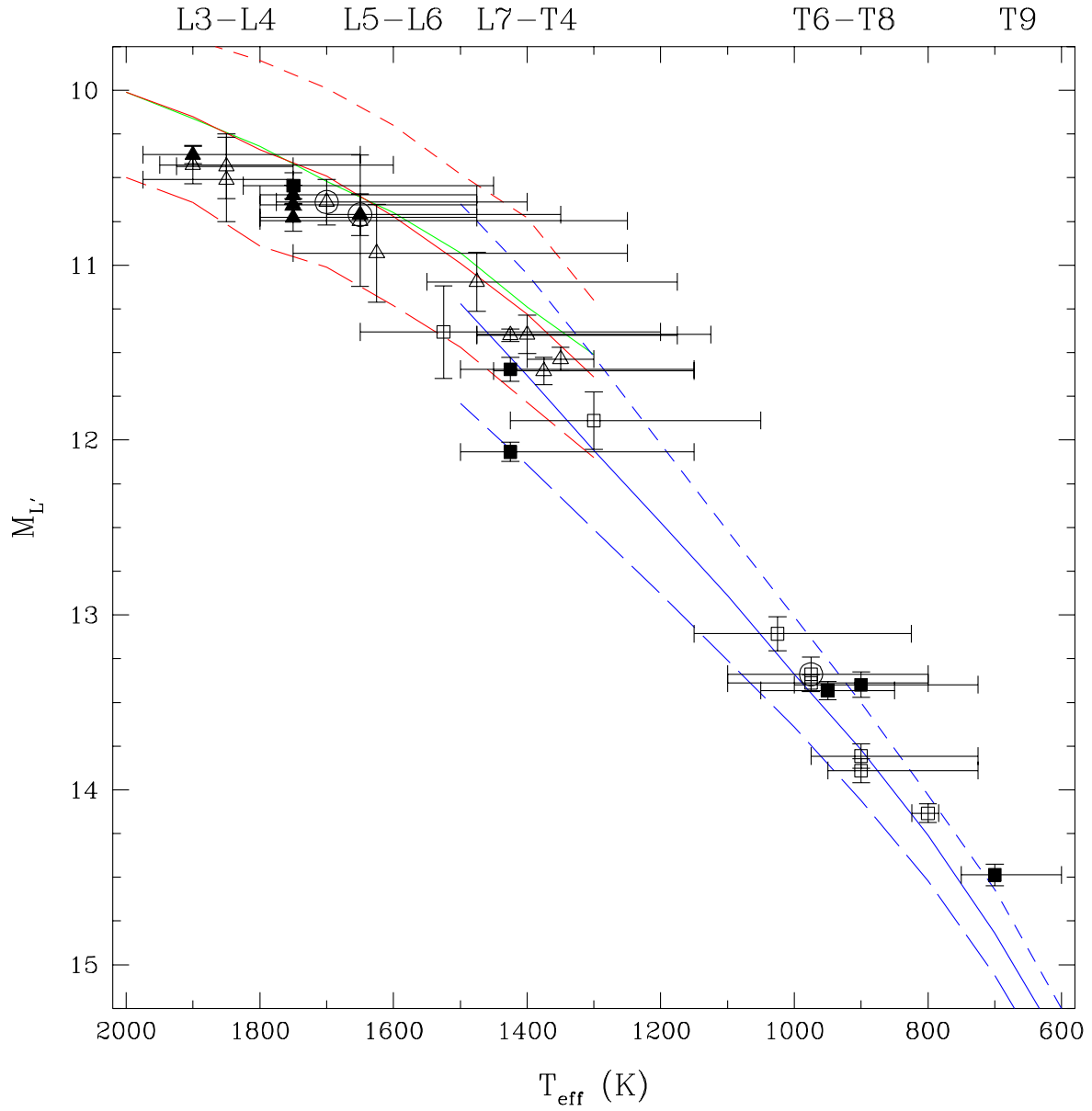


Fig. 9.— Diagram of $M_{L'}$ versus T_{eff} for L3–T9 dwarfs listed in Table 6. All symbols and curves are described in Figure 8.

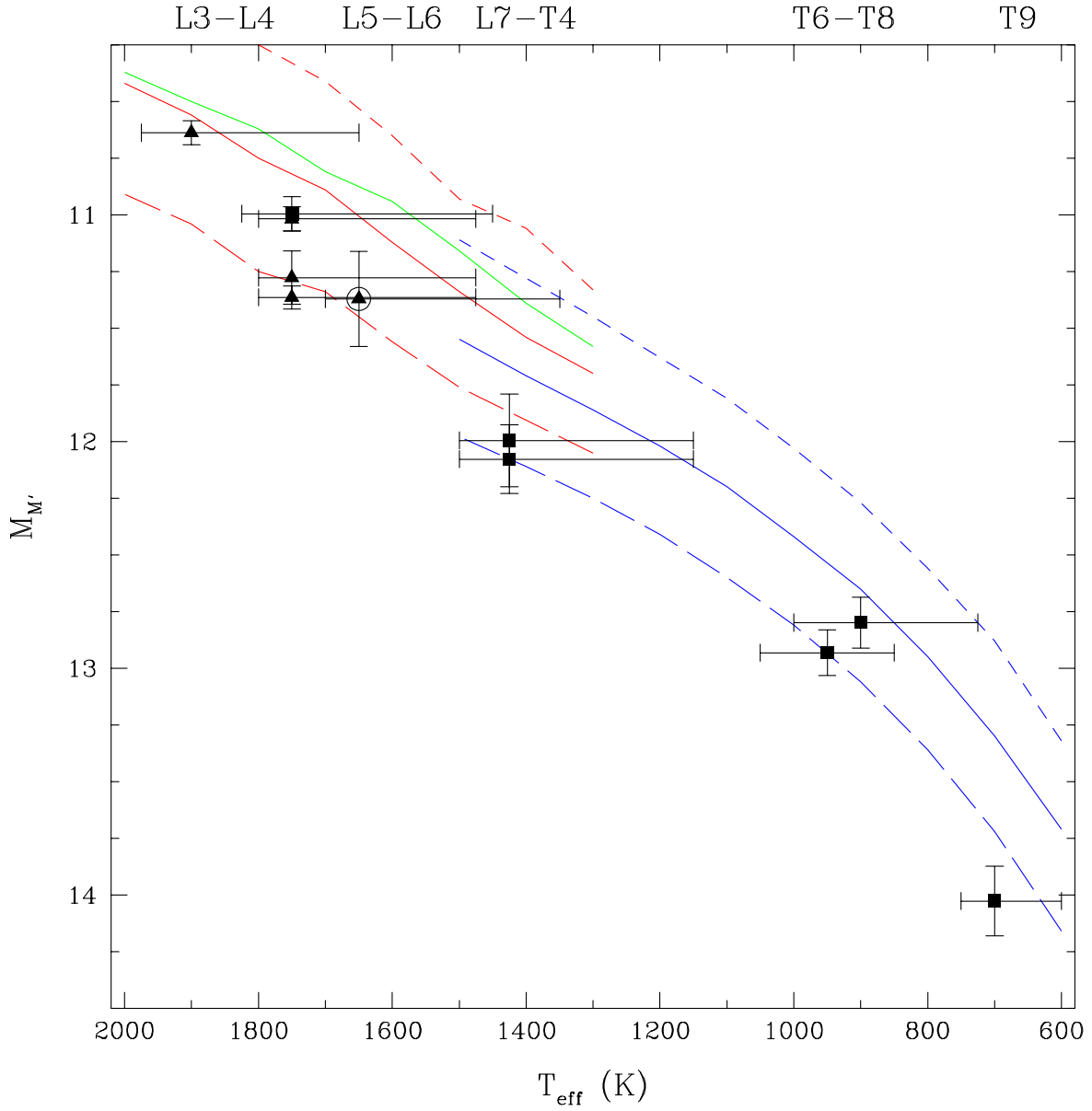


Fig. 10.— Diagram of $M_{M'}$ versus T_{eff} for L3–T9 dwarfs listed in Table 6. All symbols and curves are described in Figure 8.